Cancer Biol Med 2018. doi: 10.20892/j.issn.2095-3941.2018.0012

ORIGINAL ARTICLE

OPEN ACCESS

Enterolactone modulates the ERK/NF-κB/Snail signaling pathway in triple-negative breast cancer cell line MDA-MB-231 to revert the TGF-β-induced epithelial–mesenchymal transition

Aniket V. Mali[1,2], Asavari A. Joshi[1], Mahabaleshwar V. Hegde[1], Shivajirao S. Kadam[2]

[1]Center for Innovation in Nutrition Health and Disease (CINHD), Interactive Research School for Health Affairs (IRSHA), Bharati Vidyapeeth Deemed to be University (BVDU), Dhankawadi, Pune, Maharashtra 411043, India; [2]Pharmaceutical Sciences, Poona College of Pharmacy, Bharati Vidyapeeth Deemed to be University (BVDU), Pune, Maharashtra 411038, India

ABSTRACT

Objective: Triple-negative breast cancer (TNBC) is highly metastatic, and there is an urgent unmet need to develop novel therapeutic strategies leading to the new drug discoveries against metastasis. The transforming growth factor-β (TGF-β) is known to promote the invasive and migratory potential of breast cancer cells through induction of epithelial–mesenchymal transition (EMT) via the ERK/NF-κB/Snail signaling pathway, leading to breast cancer metastasis. Targeting this pathway to revert the EMT would be an attractive, novel therapeutic strategy to halt breast cancer metastasis.

Methods: Effects of enterolactone (EL) on the cell cycle and apoptosis were investigated using flow cytometry and a cleaved caspase-3 enzyme-linked immunosorbent assay (ELISA), respectively. Effects of TGF-β induction and EL treatment on the functional malignancy of MDA-MB-231 breast cancer cells were investigated using migration and chemo-invasion assays. The effects of EL on EMT markers and the ERK/NF-κB/Snail signaling pathway after TGF-β induction were studied using confocal microscopy, quantitative reverse transcription polymerase chain reaction (qRT-PCR), Western blot, and flow cytometry.

Results: Herein, we report that EL exhibits a significant antimetastatic effect on MDA-MB-231 cells by almost reverting the TGF-β-induced EMT *in vitro*. EL downregulates the mesenchymal markers N-cadherin and vimentin, and upregulates the epithelial markers E-cadherin and occludin. It represses actin stress fiber formation via inhibition of mitogen-activated protein kinase p-38 (MAPK-p38) and cluster of differentiation 44 (CD44). EL also suppresses ERK-1/2, NF-κB, and Snail at the mRNA and protein levels.

Conclusions: Briefly, EL was found to inhibit TGF-β-induced EMT by blocking the ERK/NF-κB/Snail signaling pathway, which is a promising target for breast cancer metastasis therapy.

KEYWORDS Enterolactone; breast cancer metastasis; EMT; invasion; migration

Introduction

The most common malignant tumor in females is breast cancer, and its metastasis is the leading cause of death in breast cancer patients[1]. At the cellular level, metastasis comprises of an orderly sequence of pathological molecular events, collectively termed the metastatic cascade that starts with the epithelial–mesenchymal transition (EMT), followed by extracellular matrix (ECM) remodeling, and the invasion of cancer cells through the basal membrane into the blood vessels (intravasation); the survival of the cancer cells in the blood stream; the departure of the cancer cells from the blood capillary and their entry into the tissues of a distant organ (extravasation); and the colonization and multiplication of the cancer cells to prosper in a new more conducive environment[2,3]. The transforming growth factor beta (TGF-β) pathway has been implicated in many of these metastatic processes, and has been shown to significantly enhance the ability of tumor cells to spread throughout the body[4]. One of the main mechanisms by which TGF-β promotes cell migration, invasion, and metastasis is through induction of EMT; thus, TGF-β has become the foremost EMT inducer in experimental studies[5]. The transcription

Correspondence to: Mahabaleshwar V. Hegde
E-mail: mahabaleshwarh@yahoo.com
Received January 19, 2018; accepted March 14, 2018.
Available at www.cancerbiomed.org

factor, nuclear factor kappa B (NF-κB), plays an essential role in breast cancer progression by inducing and maintaining EMT with the cooperation of Ras- and TGF-β-dependent signaling pathways[6]. The activation of extracellular signal-regulated kinases (ERKs) contributes to the regulation of NF-κB activity during TGF-β-induced EMT[7]. It has also been shown that ERKs and NF-κB stimulate another EMT-inducible transcription factor (Snail)[8], which functions as one of the master molecular switches of the EMT program[9]. A recent study has demonstrated that inhibition of the ERK/NF-κB/Snail signaling pathway reverses TGF-β-induced EMT in breast cancer cells[10].

EMT is the process by which epithelial cells lose cell–cell junctions and baso-apical polarity, and acquire plasticity, mobility, invasive capacity, stem-like characteristics, and resistance to apoptosis[11]. The molecular hallmark of EMT is the downregulation of the cell–cell adhesion molecule E-cadherin, which results in the dissolution of cell–cell tight junctions, the upregulation of a number of mesenchymal markers—including N-cadherin, vimentin, and fibronectin (FN)—and the reorganization of the cytoskeletal architecture via the formation of actin stress fibers and changes to cell shape[12]. The EMT process not only alters the cellular characteristics of cancer cells from the epithelial to the mesenchymal phenotype, but also triggers ECM remodeling through the activation of various proteases such as matrix metalloproteinases (MMPs) to acquire anoikis resistance, increased invasiveness, and migratory potential to promote metastasis[13]. Enterodiol (ED) and enterolactone (EL)—the mammalian lignans derived from the flax lignan—are very well known for their anti-breast cancer activity[14]. In our previous studies, we have demonstrated the antimetastatic potential of EL through its antiproliferative, antimigratory, and anti-invasive mechanisms, along with its ability to inhibit urokinase plasminogen activator (uPA)-induced plasmin activation and MMP-mediated ECM remodeling in breast cancer cells[15,16]. In the present study, we demonstrate that EL can revert TGF-β-induced EMT in MDA-MB-231 breast cancer cells *in vitro*.

Materials and methods

Reagents and materials

EL, tamoxifen (TAM), doxorubicin (DOXO), TGF-β1, Dulbecco's phosphate-buffered saline (DPBS), dimethyl sulfoxide (DMSO), propidium iodide (PI), RNase A, tetramethylrhodamine B isothiocyanate (TRITC)-phalloidin, 4′, 6-diamidino-2-phenylindole (DAPI), and an antibiotic antimycotic solution containing 10, 000 units penicillin, 10 mg streptomycin, and 25 μg amphotericin B per mL were purchased from Sigma-Aldrich (St. Louis, MO, USA). Leibovitz's L-15 Medium, trypsin–ethylenediaminetetraacetic acid (EDTA) (0.25%), and fetal bovine serum (FBS) were procured from Gibco (BRL, CA, USA). TRIzol reagent, chloroform, isopropanol, and diethyl pyrocarbonate (DEPC)-treated water were purchased from Sigma-Aldrich (St. Louis, MO, USA). A CHEMICON Cell Invasion Assay Kit was purchased from Merck Millipore (Burlington, MA, US). The quantitative reverse transcription polymerase chain reaction (qRT-PCR) kits and reagents GoScript™ Reverse Transcription System and GoTaq® qPCR Master Mix were purchased from Promega (Madison, WI, USA). Primary rabbit antibodies anti-E-cadherin, anti-vimentin, anti-MAPK-p38, anti-tubulin, anti-ERK-1/2, and anti-pERK-1/2 were purchased from Sigma-Aldrich (St. Louis, MO, USA). Primary antibody anti-NF-κB/p65 was purchased from Santa Cruz (Santa Cruz, CA, USA), whereas anti-Snail was purchased from Novus Biologicals (Littleton, CO, USA). Goat anti-rabbit secondary antibody-peroxidase, goat anti-rabbit secondary antibody-fluorescein isothiocyanate (FITC), protease inhibitor cocktail, and phosphatase inhibitor cocktail were purchased from Sigma-Aldrich (St. Louis, MO, USA). Goat anti-rabbit secondary antibody-TRITC, a Pierce Cleaved Caspase-3 Colorimetric In-Cell ELISA Kit (ELISA, enzyme-linked immunosorbent assay), and a SuperSignal™ West Femto Maximum Sensitivity Substrate Kit were purchased from Thermo Scientific (Rockford, IL, USA). The antibodies for fluorescence-activated cell sorting (FACS)—phycoerythrin (PE)-anti-human CD44, PE-mouse IgG1, and κ isotype control—were purchased from BioLegend (San Diego, CA, USA). Amicon® Ultra-4 centrifugal filters and Immobilon® polyvinylidene difluoride (PVDF) transfer membranes were purchased from Millipore (Tullagreen, Carrigtwohill, Republic of Ireland). All other common reagents were procured from HiMedia Laboratories Pvt. Ltd. (Mumbai, India).

Cell culture and treatment

Breast cancer cell line MDA-MB-231 was obtained from the National Centre for Cell Science (NCCS), Pune, India. The cells were cultured as monolayers in Leibovitz's L-15 medium supplemented with L-glutamine and sodium pyruvate, antibiotic antimycotic solution, and 10% FBS at 37°C in a humidified atmosphere without CO_2 and allowing exchange

with air . A stock solution (60 mM) was prepared by dissolving EL in absolute ethanol; the solution was stored at 4°C. Working solutions of EL were then made by serial dilution of the stock solution with cell culture medium, and ethanol was employed as a negative control at a final concentration not exceeding 0.2% (v/v) in the cell culture experiments. Similarly, a stock solution of TAM (20 mM) was prepared in DMSO and used as a negative control at a final concentration of less than 0.5% (v/v) in the cell culture experiments. TGF-β was dissolved in sterile distilled water to prepare a stock solution (10 μg/mL). Based on the half maximal inhibitory concentration (IC_{50}) of EL (73 ± 2.83 μM for 48 h)[16], in all the experiments EL treatments were continued for 48 h at various concentrations (25, 50, and 75 μM), except for the caspase-3 ELISA (15 h), cell migration assay (36 h), and cell invasion assay (24 h), whereas TGF-β induction was carried out using 10 ng/mL concentrations for 48 h.

Cell cycle analysis

MDA-MB-231 cells were seeded at a density of 0.3×10^6 cells per well in 6-well plates, and incubated overnight at 37°C in a 5% CO_2 incubator. The cells were treated with various concentrations of enterolactone (25, 50, and 75 μM), and incubated for 48 h. Following incubation, the cells were harvested by trypsinization, washed with PBS, and fixed with 70% ethanol for 1 h on ice. After washing with PBS, the cell pellet was resuspended in 0.2 mL of PI staining solution containing 100 μg/mL RNase A and 50 μg/mL PI. The cells were then incubated for 1 h at room temperature and analyzed using a BD LSRFortessa™ flow cytometer (BD Biosciences, Bedford, MA, USA). An analysis of the cell cycle was performed using FCS Express software.

Caspase-3 activity ELISA

MDA-MB-231 cells were seeded into 96-well plates at a cell density of 10000 cells per well, cultured overnight, and treated for 15 h with various concentrations of EL (25, 50, and 75 μM) and TAM (1 and 5 μM) diluted with L-15 complete medium. Caspase-3 activity was examined using a cleaved caspase-3 colorimetric in-cell ELISA Kit (Thermo Scientific, IL, USA) in accordance with the manufacturer's protocol. Absorbance at 450 nm (A_{450}) was determined using an iMark™ microplate reader (BIO-RAD, California, USA). All the A_{450} values were normalized to background measurement and the differences in cell numbers in the various wells, and caspase-3 activity was calculated as a fold change compared with the control. The results were derived from at least three independent sets of triplicate experiments.

Cell migration assay

The effects of EL on the migration potential of MDA-MB-231 breast cancer cells when stimulated with TGF-β were analyzed using a cell migration assay. The MDA-MB-231 cells were seeded at a density of 0.3×10^6 cells per well in 6-well plates, and incubated overnight at 37°C in a 5% CO_2 incubator. An artificial wound was made with a sterile tip. Detached cells were removed by discarding the existing media and replacing it with fresh media containing various concentrations of EL (25, 50, and 75 μM) in the presence and absence of TGF-β (10 ng/mL), or ethanol alone as a negative control. The speed of wound closure and cell migration was quantified by taking snapshot pictures with an inverted microscope (Magnus-INVI, New Delhi, India) at 0-, 20-, and 36-h time intervals. To determine the statistical significance of the data, we carried out automated analysis of the monolayer wound-healing assay by processing the images using a computational tool (TScratch software), as described elsewhere[17].

Cell invasion assay

The cell invasion assay was carried out by using a CHEMICON Cell Invasion Assay Kit (Merck Millipore, MA, US) in accordance with the manufacturer's protocol. Briefly, a cell suspension containing 0.5 to 1×10^6 cells/mL in serum-free medium was prepared, and 300 μL of this prepared cell suspension was added to each rehydrated cell insert. A medium containing 10% FBS (500 μL) was added to each lower chamber. The cells were incubated for 24 h with various concentrations of EL (25, 50, and 75 μM) in the presence and absence of TGF-β (10 ng/mL), or ethanol alone as a negative control. After incubation, the non-invading cells and ECM gel were removed from the interior of the inserts using cotton-tipped swabs. Invasive cells were further stained and photographed using an inverted microscope (Magnus-INVI, New Delhi, India) under 4X magnification. Additionally, invasive cells were quantified colorimetrically at 560 nm by dissolving the stained cells in 10% acetic acid.

Immunofluorescence staining

The MDA-MB-231 cells were seeded in 6-well plates with cover slips at a density of 0.3×10^6 per well, and cultured at 37°C. When they reached ~60% confluence, the cells were

further treated with various concentrations of EL (25, 50, and 75 μM) and TAM (0.5 μM) 1 h before TGF-β induction. TGF-β induction was carried out by adding 10 ng/mL of TGF-β solution to each well. After 48 h of treatment and induction, the cells with or without EL treatment and TGF-β induction were first washed three times with PBS and then fixed with 4% paraformaldehyde for 20 min at room temperature (RT). After permeabilization with 0.1% Triton X-100, the cells were blocked with 5% bovine serum albumin (BSA) for 1 h, and subsequently incubated with primary antibodies anti-E-cadherin (1:500 dilution) and anti-vimentin (1:400 dilution) overnight at 4°C. After washing with PBS, the cells were incubated with goat anti-rabbit IgG-FITC and goat anti-rabbit IgG-TRITC secondary antibodies for E-cadherin and vimentin, respectively, in the dark for 1 h at RT. The cells were further washed with PBS to remove excess antibodies, and counterstained with DAPI. The cover slips were then mounted and fixed on microscope slides and processed for imaging on a Zeiss LSM510 META advanced spectral confocal microscope (Oberkochen, Germany).

After 48 h of EL treatment and TGF-β induction, the cells were fixed with 4% paraformaldehyde for 20 min to prepare them for actin stress fiber staining. After permeabilization with 0.1% Triton X-100, the cells were stained with a 50 μg/mL fluorescent phalloidin conjugate solution in PBS for 40 min at RT. The cells were further washed with PBS to remove excess unbound phalloidin conjugate, and counterstained with DAPI. The cover slips were then mounted and fixed on microscope slides, and processed for imaging on an advanced spectral confocal microscope.

FACS analysis of CD44 expression

The MDA-MB-231 cells were seeded in 6-well plates at a density of 0.3×10^6 per well, and cultured overnight at 37°C. The cells were further treated with various concentrations of EL (25, 50, and 75 μM) and TAM (0.5 μM) 1 h before TGF-β induction. TGF-β induction was carried out by adding 10 ng/mL of TGF-β solution to each well. After 48 h of treatment, the cells were trypsinized, collected in PBS, and pellets were formed at a relative centrifugal force (RCF) of 720. The cells were then sieved through 40 μm cell strainers to obtain a single cell suspension. The cell pellets were resuspended in a cell-staining buffer containing 1% BSA in PBS at a density of 10^6 cells per 100 μL. All the samples were further stained with 5 μL each of PE-anti-human CD44, PE mouse IgG1, κ isotype control by incubating at 4°C for 30 min in the dark. After washing with PBS, the cells were resuspended in cell-staining buffer and transferred to pre-labeled FACS tubes on ice. All the samples were further analyzed by FACS using a BD LSRFortessa™ flow cytometer (BD Biosciences, Bedford, MA). All the necessary precautions, such as using the same number of cells, the same concentration of staining antibody, and the same staining volume, were taken during the experiment and the fluorescence was recorded in the PE channel by stringently gating the cell population to avoid dead/apoptotic cells. The unstained control and the isotype control were also included in the experiment to eliminate the background readings due to auto fluorescence and non-specific binding, and the results were represented as median fluorescence intensity and mean fluorescence intensity (MFI).

Quantitative reverse transcription polymerase chain reaction (qRT-PCR)

After treatment with 25, 50, and 75 μM of EL and 0.5 μM of TAM and TGF-β induction for 48 h, total RNA was isolated using TRIzol reagent in three independent experiments. The purity and concentration of the isolated RNA were measured using a BioPhotometer® Plus system (Eppendorf, Hamburg, Germany). First strand complementary DNA (cDNA) synthesis was performed using a GoScript™ Reverse Transcription System (Promega, Madison, USA), according to the manufacturer's protocol. The human oligonucleotide primers were synthesized by Eurofins Genomics India Pvt. Ltd. (Bangalore, India) for the multiple genes under investigation, as illustrated in **Table S1**. Afterwards, qRT-PCR was carried out using a GoTaq® qPCR Master Mix (Promega, Madison, USA), as per the manufacturer's protocol, on a StepOne™ Real-Time PCR System (Applied Biosystems, California, USA). The expression of each gene was assayed using three replicates for each primer along with a glyceraldehyde 3-phosphate dehydrogenase (GAPDH) primer as an internal standard and negative control lacking the cDNA template. The analysis of the qRT-PCR gene expression data was carried out using a relative quantification method, and changes in gene expression were presented using the comparative CT method ($2^{-\Delta\Delta CT}$ method), as described in the literature[18].

Western blot

After treatment with 25, 50, and 75 μM of EL and 0.5 μM of TAM and TGF-β induction for 48 h, the cells were lysed with NP-40 buffer, and protein levels in the cell lysates were measured using a standard Bradford assay. Total proteins (30 μg) were separated on 10% sodium dodecyl sulfate–

polyacrylamide electrophoresis gels, and transferred to PVDF membranes (Millipore, Tullagreen, Republic of Ireland) using a Trans-Blot SD Semi-Dry Transfer Cell (BIO-RAD, California, USA). After blocking with 5% BSA in tris-buffered saline and Tween-20 (TBST), the membranes were separately incubated overnight at 4°C with antibodies for vimentin, E-cadherin, MAPK-p38, NF-κB/p65, tERK-1/2, pERK-1/2, Snail, and tubulin. The membranes were then washed and incubated with horseradish peroxidase-conjugated secondary antibodies for 1 h. The bands were detected using a SuperSignal West Femto Maximum Sensitivity Substrate Kit (Thermo Scientific, Rockford, USA) using a ChemiDoc™ XRS+ System with Image Lab™ Software (BIO-RAD, California, USA).

Statistical analysis

All the experiments were performed in triplicate and repeated thrice. The data are presented as the mean ± SEM. Statistical analysis was performed with the GraphPad Prism 5 program, and differences between groups were examined for statistical significance using one-way analysis of variance (ANOVA) followed by Tukey's multiple comparison test; independent samples were analyzed using the *t*-test. $P < 0.05$ was considered statistically significant.

Results

EL arrested the growth of MDA-MB-231 breast cancer cells in the 'S' phase

The effects of EL on the cell cycle of MDA-MB-231 cells were determined using flow cytometry after 48 h of treatment. EL induced an accumulation of cells in the 'S' phase with corresponding decrease in the cell population in the 'G2' phase in a dose-dependent manner (**Figure 1A**). There was a non-significant increase (~24%) in the S phase population following treatment with 25 μM EL, whereas there were significant increases (~34% and ~39%) following treatment with 50 and 75 μM EL, respectively ($P \leq 0.001$), compared with the untreated cells (~17%). The results were also compared with those of anti-breast cancer drugs as positive controls: with one known for G1 arrest; Tamoxifen (TAM), and another known for G2 arrest; Doxorubicin (DOXO) in MDA-MB-231 breast cancer cells TAM treatment (5 μM) caused significant cell arrest in the G1 phase (~72%; $P \leq 0.001$) compared with the untreated cells in G1 (~55%), and DOXO treatment (100 nM) caused significant cell arrest in the G2 phase (~92%; $P \leq 0.001$) compared with the untreated cells in G2 (~27%) (**Figure S1**).

EL triggered apoptosis in MDA-MB-231 breast cancer cells via caspase-3 activation

Considering the central role caspase-3 plays in executing apoptosis in breast cancer, we next determined the effects of EL on caspase-3 activation, which is known to cleave poly (ADP-ribose) polymerase (PARP) and other proteins leading to apoptosis[19]. After 15 h of treatment, the protein levels of cleaved caspase-3 were determined by ELISA. As shown in **Figure 1B**, there was a significant ~1.6-fold increase in the level of cleaved caspase-3 when 25 μM EL was used ($P \leq 0.01$) and significant ~1.8- and ~2.1-fold increases when 50 and 75 μM EL were used, respectively ($P \leq 0.001$), compared with the untreated cells. TAM (the positive control) also caused a significant ~1.6-fold increase in the level of cleaved caspase-3 when used at a concentration of 1 μM, and a ~2.1-fold increase when used at a concentration of 5 μM.

EL inhibited TGF-β-induced migration of MDA-MB-231 breast cancer cells

To examine the effect of EL on TGF-β-induced cell migration in metastatic breast cancer cells, we performed a wound-healing assay on confluent monolayers of MDA-MB-231 cells. After making the wound with a pipette tip, the cells were cultured in the presence or absence of TGF-β and various concentrations of EL, and imaged using an inverted microscope at intervals of 0, 20, and 36 h. EL effectively inhibited the migration of TGF-β-stimulated cells in a dose-dependent manner at all time-points studied compared with only TGF-β-stimulated cells (**Figure 1C** and **1D**). The images were processed using a computational tool (TScratch software) to quantify the open wound area as a "mean % open wound area", and plotted as shown in **Figure 1D**. In the untreated control cells there was ~47% and ~64% reduction in the open wound area following treatment for 20 h and 36 h, respectively. In contrast, in the TGF-β-stimulated cells there was a significant increase in migration compared with the untreated control cells, shown by ~68% ($P \leq 0.01$) and ~78% ($P \leq 0.05$) reductions in the open wound area following treatment for 20 h and 36 h, respectively, which can be attributed to TGF-β induction. Conversely, there was a significant dose-dependent decrease in cell migration at EL concentrations of 25 ($P \leq 0.01$), 50 ($P \leq 0.001$), and 75 μM ($P \leq 0.001$) quantified as reductions in the mean % open wound area of ~45%, ~35%, and ~22%, respectively, at 20 h, whereas there were reductions of ~57%, ~48%, and ~28% at 36 h, respectively, compared with only TGF-β-stimulated cells. Thus, EL was confirmed to have the potential to inhibit

the TGF-β-induced migration of metastatic MDA-MB-231 breast cancer cells *in vitro* in a dose- and time-dependent manner.

EL inhibited TGF-β-induced invasion of MDA-MB-231 breast cancer cells through ECM

To study the effect of EL on TGF-β-induced cell invasion through ECM in metastatic breast cancer cells, we performed a cell invasion assay on MDA-MB-231 cells in an invasion chamber with cell culture inserts of pore size 8 μm, over which a thin layer of ECM was dried. The cells were seeded in the inserts and treated for 24 h with various concentrations of EL in the presence and absence of TGF-β (10 ng/mL). EL significantly inhibited the invasion of TGF-β-stimulated cells in a dose-dependent manner after 24 h, compared with only

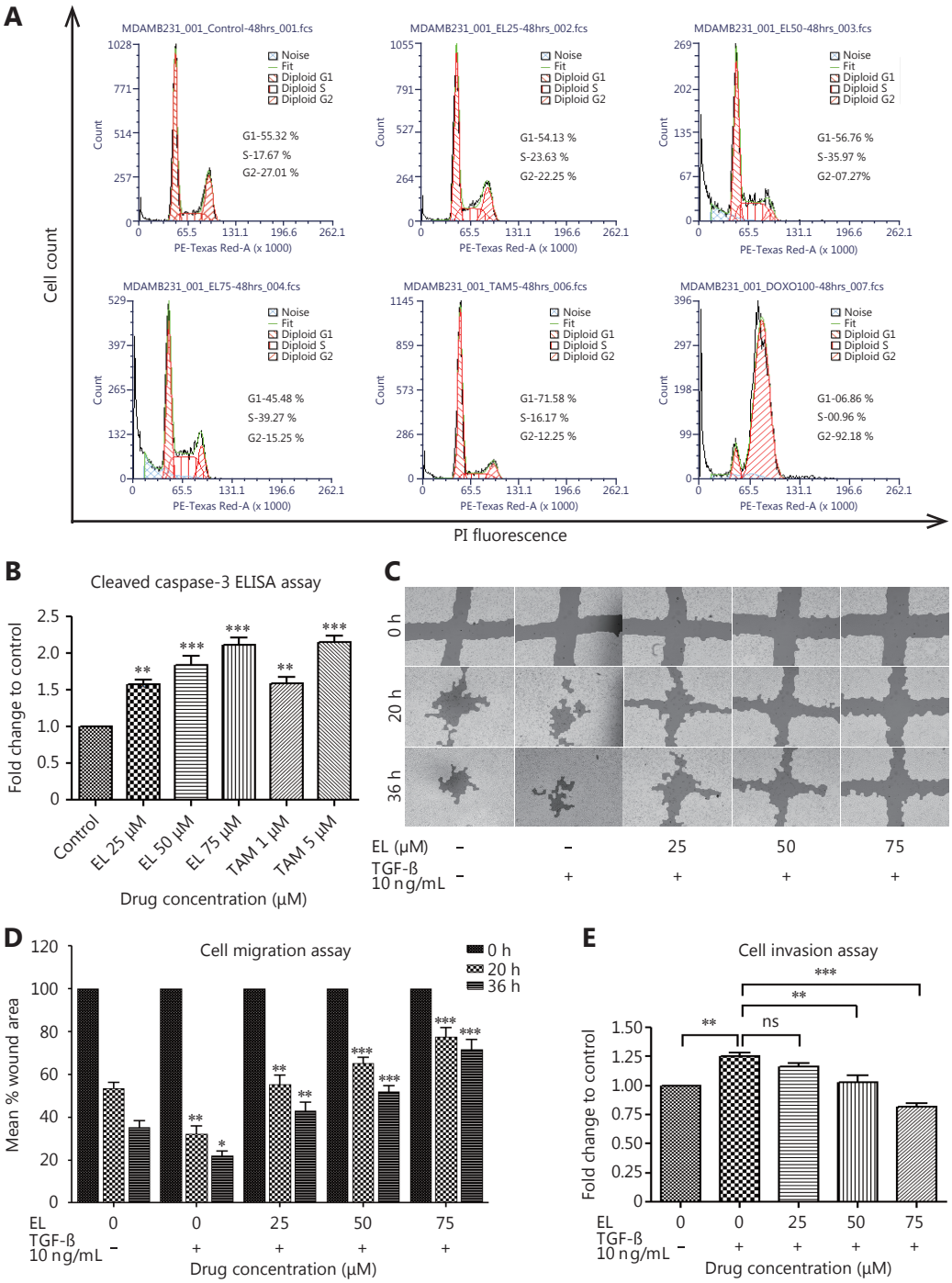

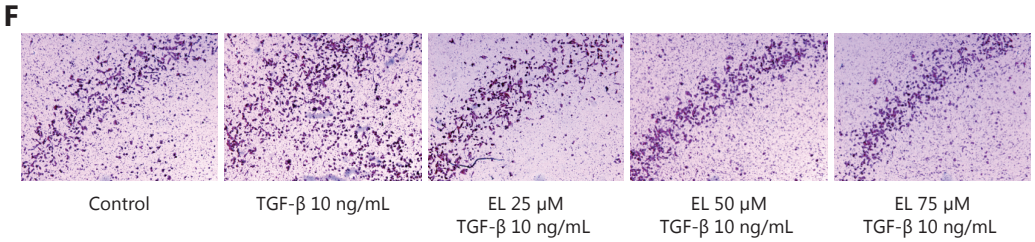

Figure 1 Effects of EL on the cell cycle, caspase-3 activity, migration, and invasion of MDA-MB-231 breast cancer cells. (A) Representative histograms of flow cytometry analysis indicating dose-dependent "S" phase arrest after EL treatment. (B) Increased activity of cleaved caspase-3 in MDA-MB-231 cells when concentrations of 25, 50, and 75 μM EL were used. (C) Increased migration of MDA-MB-231 cells after transforming growth factor beta (TGF-β) stimulation (10 ng/mL), and decreased migration when concentrations of 25, 50, and 75 μM EL were used. The images were obtained using an inverted microscope with a 4 × objective at 0-, 20-, and 36-h time intervals, and were processed using a computational tool (TScratch software). The original unprocessed images are shown in supplementary files. (D) Quantification of a time-dependent increase in cell migration after TGF-β stimulation, and a dose-dependent decrease in cell migration after EL treatment, using TScratch software. The analyzed data are represented graphically as mean % open wound area versus EL dose at 0-, 20-, and 36-h time intervals. (E) Quantification of the increase in cell invasion through the ECM after TGF-β stimulation, and the dose-dependent decrease in cell invasion after EL treatment. (F) Increased invasion of MDA-MB-231 cells through the ECM after TGF-β stimulation (10 ng/mL), and decreased invasion when concentrations of 25, 50, and 75 μM EL were used. The images were obtained using an inverted microscope with a 4 × objective at 24-h time intervals. Values are represented as mean ± SEM of three independent experiments (n = 3), with *$P \leq 0.05$, **$P \leq 0.01$, and ***$P \leq 0.001$ indicating statistical significance.

TGF-β-stimulated cells (**Figure 1E** and **1F**). The invasive cells were quantified colorimetrically by dissolving the stained cells in 10% acetic acid. A significant increase of 1.26-fold ($P \leq 0.01$) was observed in the invasion of TGF-β-stimulated cells compared with the untreated control cells. However, EL significantly reduced the invasion of TGF-β-stimulated cells to ~1.16-, ~1.03- ($P \leq 0.01$), and 0.82-fold ($P \leq 0.001$) with 25, 50, and 75 μM EL treatments, respectively, compared with only TGF-β-stimulated cells. Images of the stained invasive cells were also obtained using an inverted microscope, and are presented as photographic evidence in **Figure 1F**. In conclusion, EL was found to inhibit the TGF-β-induced invasion of MDA-MB-231 breast cancer cells through ECM in a dose-dependent manner.

EL inhibited the TGF-β-induced EMT program in MDA-MB-231 breast cancer cells

A range of subtoxic EL concentrations (25, 50, and 75 μM) was chosen for the EMT-related experiments. First, we observed the morphological change indicative of EMT in MDA-MB-231 cells after TGF-β treatment. As shown in **Figure 2A**, TGF-β-induced MDA-MB-231 cells undergoing EMT acquired fibroblast-like mesenchymal morphology, and EL treatment for 48 h reverted this morphological change in a dose-dependent manner by retaining a more epithelial-like appearance, even when induced by TGF-β. The reversal of EMT changes by EL was further confirmed by studying the effects of EL on the expression patterns of epithelial markers E-cadherin and occludin, and mesenchymal markers vimentin and N-cadherin by immunofluorescence staining (confocal microscopy), qRT-PCR, and Western blot. The immunofluorescence staining data revealed that EL upregulated the expression of epithelial marker E-cadherin (**Figure 2B**), and downregulated the expression of mesenchymal marker vimentin (**Figure 2C**) in TGF-β-stimulated cells. These findings were reconfirmed by Western blot: the TGF-β-stimulated cells significantly reduced the protein expression of E-cadherin to ~0.7-fold ($P \leq 0.001$) compared with the untreated cells, whereas EL significantly increased E-cadherin expression in TGF-β-stimulated cells to ~1.21-, ~1.23-, and 1.15-fold with 25, 50, and 75 μM EL treatments, respectively ($P \leq 0.001$), compared with only TFG-β-stimulated cells (**Figure 3A**). Furthermore, there was a significant ~1.34-fold increase ($P \leq 0.001$) in the expression of vimentin protein after TGF-β stimulation compared with the untreated cells, whereas there were significant decreases in vimentin expression of ~0.93-, 0.89-, and 0.75-fold in the TGF-β-stimulated cells that had been treated with 25, 50, and 75 μM EL, respectively ($P \leq 0.001$), compared with the only TGF-β-stimulated cells (**Figure 3B**). Although no significant change in E-cadherin expression was observed following TAM treatment, treatment with 0.5 μM TAM significantly reduced vimentin expression in TGF-β-stimulated cells to

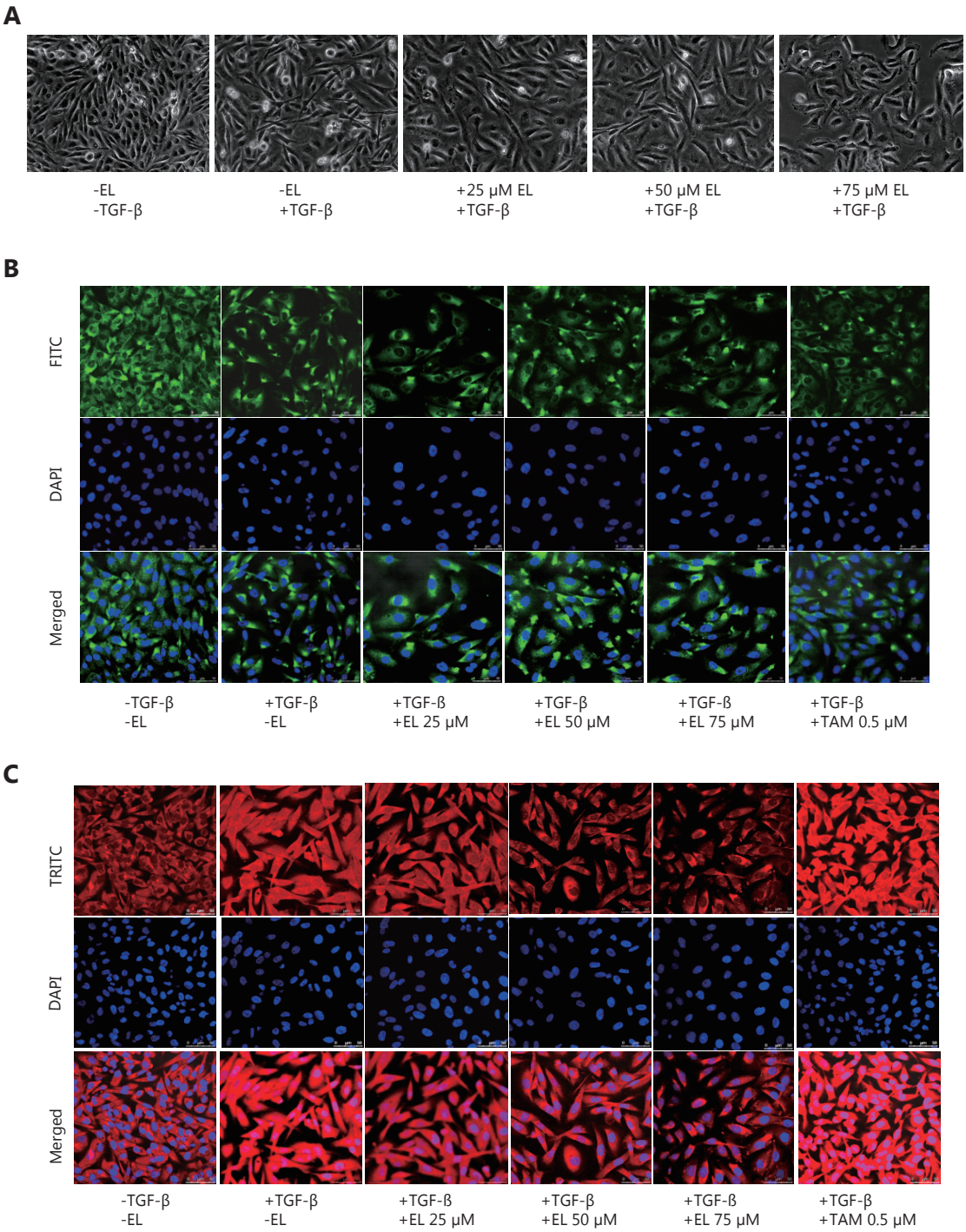

Figure 2 Confocal microscopy images of immunofluorescence staining showing the effects of EL. (A) Induction of EMT by TGF-β (10 ng/mL) characterized by fibroblast-like mesenchymal morphology, which was reverted in a dose-dependent manner by EL by retaining a more epithelial-like appearance. (B) Decreased expression of E-cadherin after TGF-β stimulation (10 ng/mL), and increased expression of E-cadherin when concentrations of 25, 50, and 75 μM EL were used. (C) Increased expression of vimentin after TGF-β stimulation (10 ng/mL), and decreased expression of vimentin when concentrations of 25, 50, and 75 μM EL were used. Values are represented as mean ± SEM of three independent experiments (n = 3), with *$P \leq 0.05$, **$P \leq 0.01$, and ***$P \leq 0.001$ indicating statistical significance.

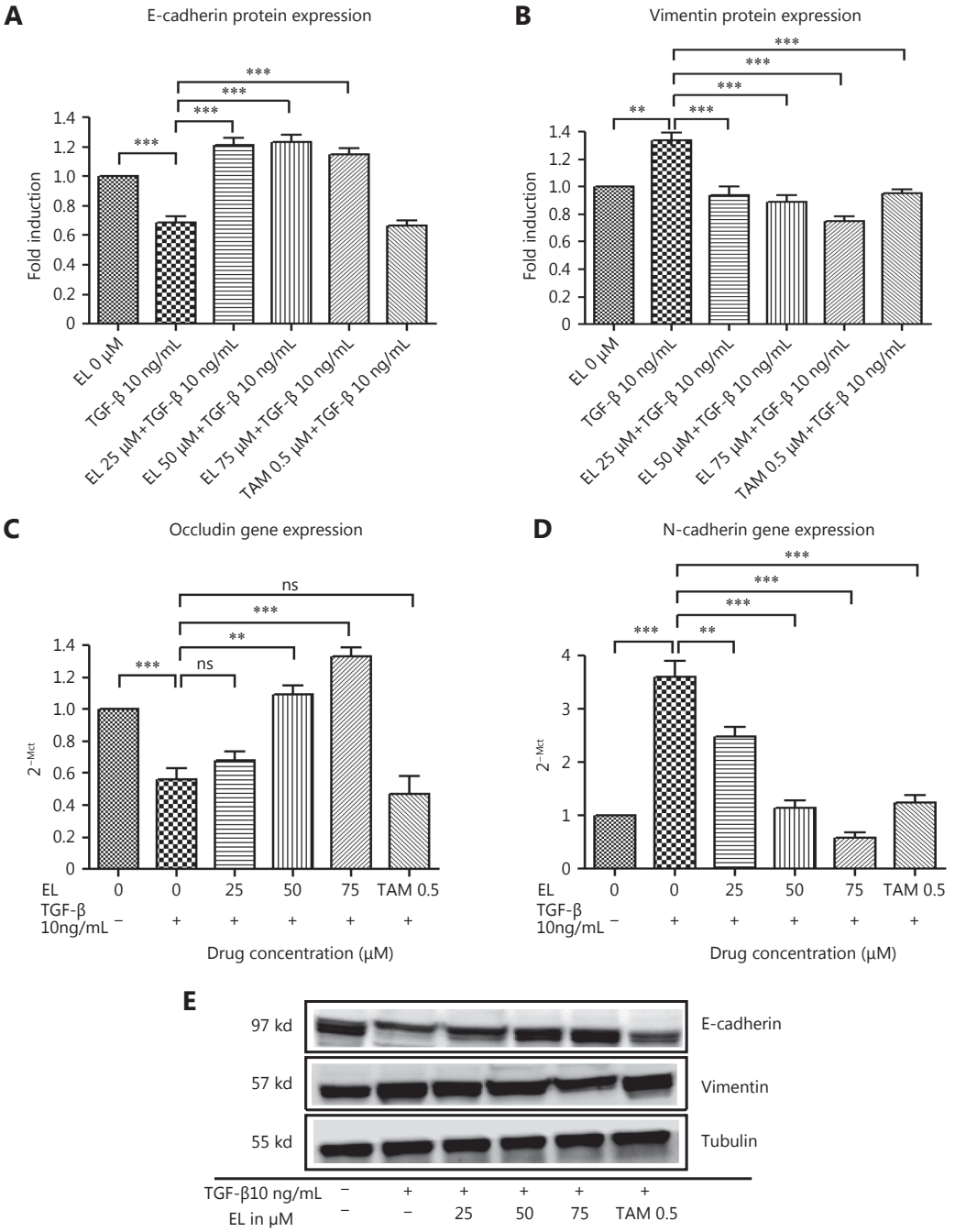

Figure 3 Effects of EL on epithelial markers E-cadherin and occludin, and mesenchymal markers vimentin and N-cadherin at the mRNA and protein levels. (A) Dose-dependent reversal of decreased expression of E-cadherin after TGF-β induction when concentrations of 25, 50, and 75 μM EL were used. (B) Dose-dependent reversal of increased expression of vimentin after TGF-β induction when concentrations of 25, 50, and 75 μM EL were used. (C) Decreased occludin gene expression after TGF-β stimulation, and increased occludin gene expression when concentrations of 25, 50, and 75 μM EL were used. (D) Increased gene expression of N-cadherin after TGF-β stimulation, and decreased gene expression of occludin when concentrations of 25, 50, and 75 μM EL were used. (E) Representative Western blot results of the indicated EMT-related proteins derived from cells treated with TGF-β (10 ng/mL) alone or combined with EL (25, 50, and 75 μM). Images of the full-length Western blot gels are shown in supplementary files. Values are represented as mean ± SEM of three independent experiments (n = 3), with *P ≤ 0.05, **P ≤ 0.01, and ***P ≤ 0.001 indicating statistical significance.

~0.96-fold ($P \leq 0.001$), compared with only TGF- β -treated cells. The expression levels of another epithelial marker (occludin) and a mesenchymal marker (N-cadherin) were also studied to confirm the reversal of EMT. As shown in **Figure 3C**, TGF-β significantly reduced the mRNA levels of occludin to ~0.56-fold compared with the untreated cells, and EL treatment significantly increased the mRNA levels of occludin in a dose-dependent manner: 50 μM (~1.09-fold; $P \leq 0.01$) and 75 μM (~1.33-fold; $P \leq 0.001$), even after TGF-β stimulation, compared with only TGF- β-stimulated cells. A significant increase in N-cadherin mRNA levels of ~3.5-fold ($P \leq 0.001$) was observed in the TGF-β-treated cells compared with the untreated cells. In contrast, EL significantly reduced the mRNA levels of N-cadherin to ~2.5-, ~1.1-, and ~0.6-fold with 25, 50 and 75 μM of EL treatment, respectively, compared with the only TGF-β-treated cells (**Figure 3D**). Briefly, EL reversed the TGF-β-induced EMT in MDA-MB-231 breast cancer cells by upregulating the epithelial markers and downregulating the mesenchymal markers.

EL reduced the formation of actin stress fibers by inhibiting the expression of CD44 and MAPK-p38

We also investigated the effects of EL on one of the important hallmarks of EMT—actin stress fiber formation—by considering the important roles played by CD44 and MAPK-p38 proteins therein. Immunofluorescence staining observed by confocal microscopy revealed that EL significantly reduced the formation of actin stress fibers in a dose-dependent manner following TGF-β stimulation (**Figure 4**), whereas TAM had no such effect. CD44 expression levels were studied using qRT-PCR and FACS analysis. The single fluorescence FACS analysis data represent the results of the various treatments versus the MFI and/or median fluorescence intensity results for the PE-stained CD44 proteins expressed in MDA-MB-231 cells. As shown in **Figure 5A**, there was significant increase ($P \leq 0.01$) in CD44 expression in the TGF-β-stimulated cells compared with the untreated cells, whereas there was a significant decrease in CD44 expression when 25, 50, or 75 μM EL was applied ($P \leq 0.001$) along with TGF-β induction, compared with only TGF-β-treated cells. Similar results were observed for the mRNA levels of CD44; TGF-β significantly increased the CD44 gene expression to ~6.5-fold ($P \leq 0.001$) compared with the untreated cells, whereas EL significantly decreased CD44 gene expression to ~3.8-, ~2.4-, and ~1-fold when 25, 50, and 75 μM EL was used ($P \leq 0.001$), even when induced by TGF-β, compared with only TGF-β-stimulated cells (**Figure 5C**). TAM treatment (0.5 μM) also significantly reduced CD44 protein expression ($P \leq 0.01$) as well as CD44 gene expression (~1.1-fold) ($P \leq 0.001$), compared with the TGF-β-stimulated cells. The expression of MAPK-p38 was also studied by qRT-PCR and Western blot. As shown in **Figure 5D**, a significant increase in MAPK-p38 gene expression (~2.1-fold; $P \leq 0.001$) was observed in the TGF-β-stimulated cells, compared with the untreated cells. However, treatment with EL at concentrations of 25, 50, and 75 μM significantly decreased MAPK-p38 gene expression to ~1.3-, ~1-, and ~0.7-fold, respectively ($P \leq 0.001$), compared with only TGF-β-treated cells. Similarly, there was a significant increase (~1.4-fold) in MAPK-p38 protein expression ($P \leq 0.05$) after TGF-β stimulation, compared with the untreated cells. The maximum activity of EL in the form of reduced protein expression (~0.7-fold) was observed at a concentration of 25 μM ($P \leq 0.001$), compared with only TGF-β-treated cells (**Figure 5E**). TAM also caused significant decreases in both gene expression (~1-fold; $P \leq 0.001$) and protein expression (~0.9-fold; $P \leq 0.01$), compared with only TGF-β- treated cells.

EL inhibited the ERK/NF-κB/Snail signaling pathway to revert TGF-β-induced EMT in MDA-MB-231 cells

Considering the ERK/NF-κB/Snail pathway as a promising therapeutic target to inhibit TGF-β-induced EMT in breast cancer cells, we investigated the effects of EL on this signaling pathway using qRT-PCR and Western blot. As shown in **Figure 6A**, TGF-β stimulation significantly increased the gene expression of ERK-1 to ~2.2-fold ($P \leq 0.001$) compared with the untreated cells, whereas EL significantly reduced gene expression to ~1.3-, 0.9-, and 0.6-fold when concentrations of 25, 50, and 75 μM EL were used, respectively ($P \leq 0.001$), even after TGF-β stimulation, compared with only TGF-β-treated cells. Similar results were observed in the case of ERK-2 gene expression (**Figure 6B**), where there was a very significant increase of ~3.7-fold following TGF-β stimulation ($P \leq 0.001$) compared with the untreated cells, and EL significantly reduced gene expression to ~3.1-, ~1.7-, and ~0.9-fold when concentrations of 25 μM ($P \leq 0.05$), 50, and 75 μM EL were used, respectively ($P \leq 0.001$), compared with only TGF-β-treated cells. A positive control (TAM) also significantly reduced the gene expression levels of both ERK-1 (~0.8-fold; $P \leq 0.001$) and ERK-2 (~0.7-fold; $P \leq 0.001$) compared with only TGF-β-treated cells. As shown in **Figure 6C**, TGF-β stimulation resulted in a significant increase (~2.4-fold; $P \leq 0.001$) in NF-κB/p65 gene expression

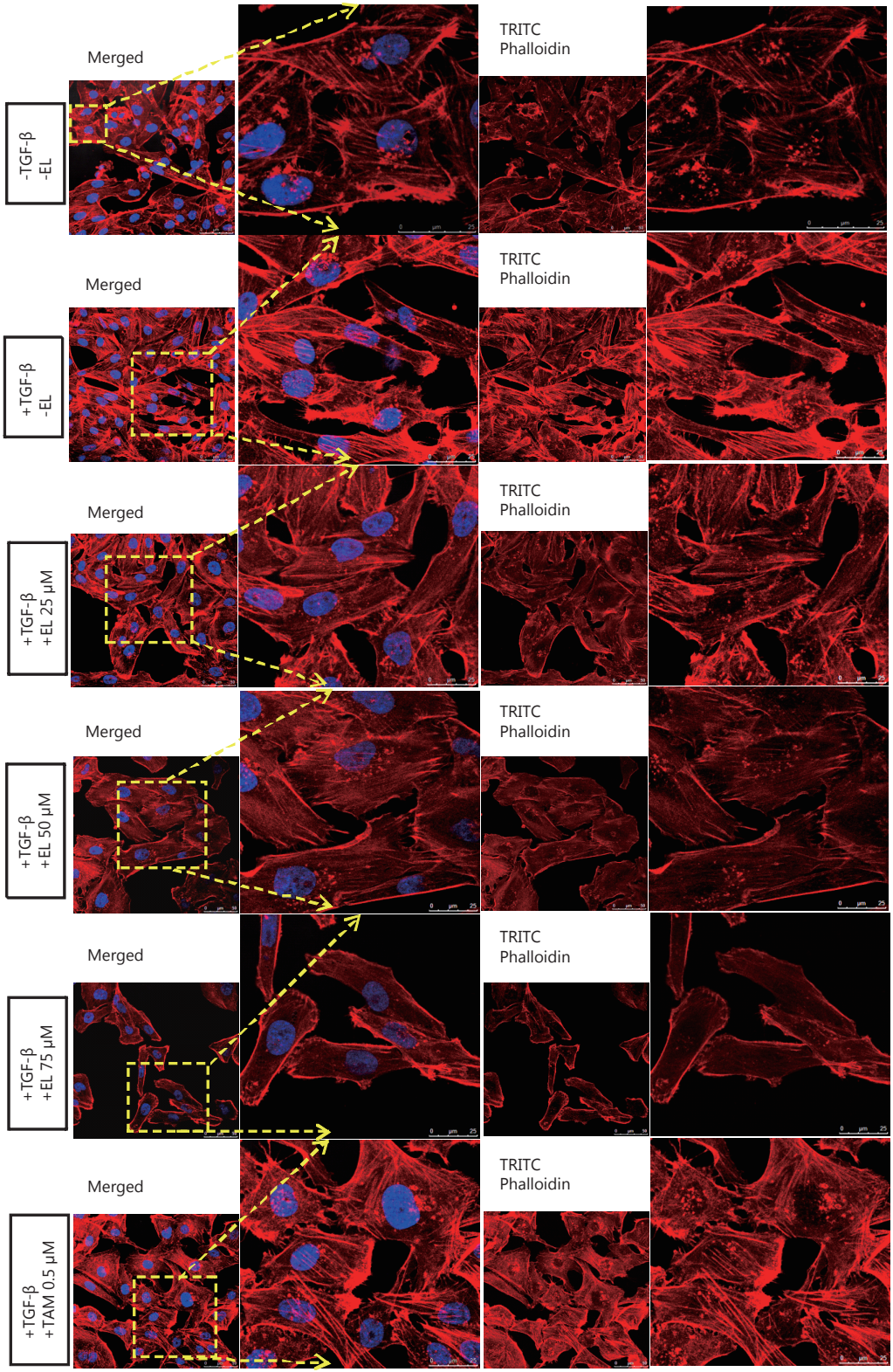

Figure 4 Effects of EL on the formation of actin stress fibers. TGF-β stimulation (10 ng/mL for 48 h) resulted in increased actin stress fiber formation, while EL treatment with 25, 50 and 75 μM for 48 h, actin stress fiber formation decreased in a dose-dependent manner.

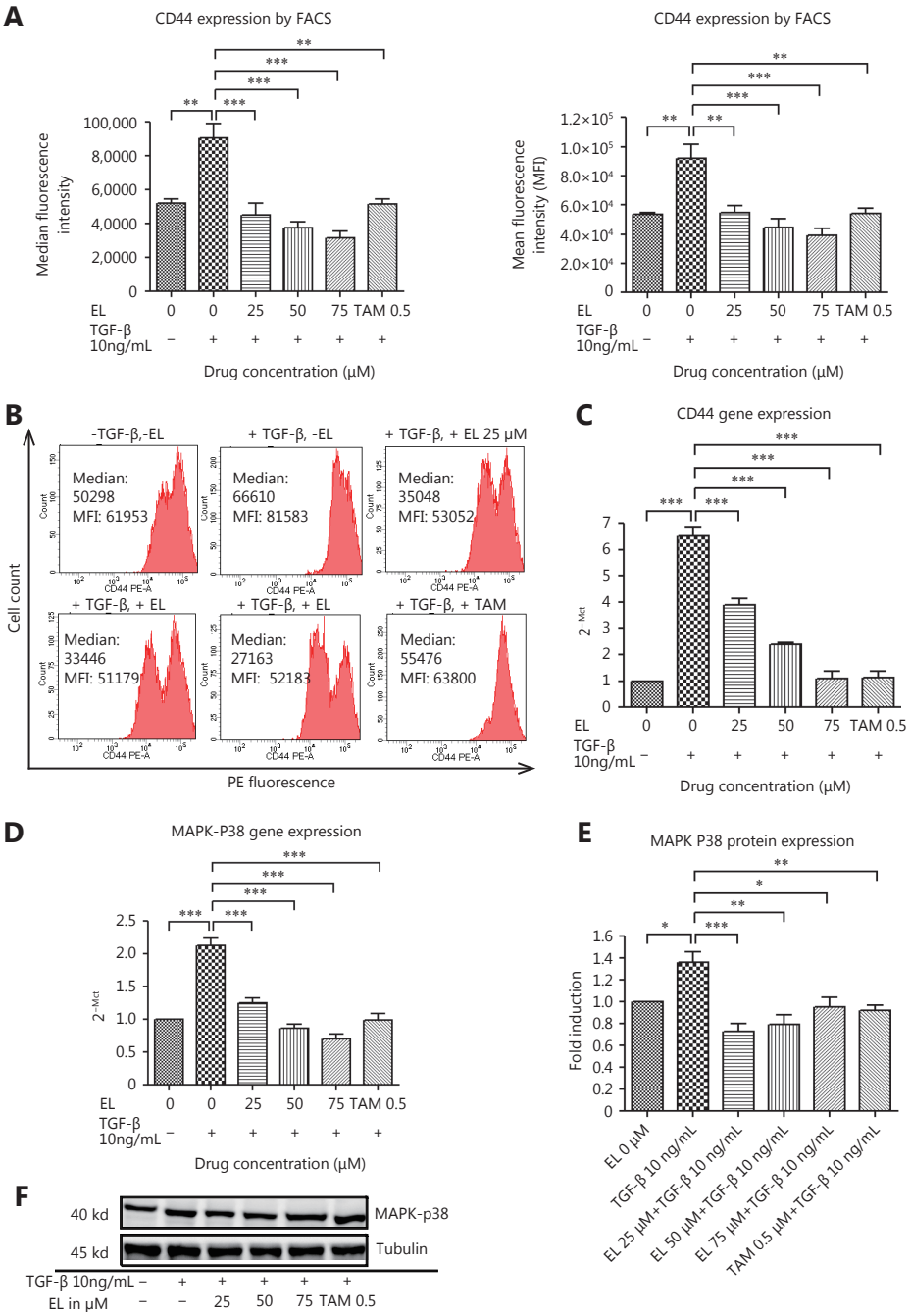

Figure 5 Effects of EL on CD44 and MAPK-p38 expression at the mRNA and protein levels. (A) Increased protein expression of CD44 after transforming growth factor beta (TGF-β) stimulation (10 ng/mL), and decreased CD44 expression with 25, 50, and 75 μM of EL treatments, indicated by median fluorescence intensity and mean fluorescence intensity (MFI). (B) Representative histograms of fluorescence-activated cell sorting (FACS) analysis indicating changes in CD44 expression in terms of MFI and median fluorescence intensity after EL treatment. (C) Increased gene expression of CD44 after TGF-β stimulation, and dose-dependent reduction in CD44 gene expression when concentrations of 25, 50, and 75 μM EL were used. (D) Increased gene expression of MAPK-p38 after TGF-β stimulation, and decreased MAPK-p38 gene expression with 25, 50, and 75 μM of EL treatments, in a dose dependent manner. (E) Increased protein expression of MAPK-p38 after TGF-β stimulation, and decreased MAPK-p38 protein expression with 25, 50, and 75 μM of EL treatments. (F) Representative Western blot results for the MAPK-p38 protein derived from cells treated with TGF-β (10 ng/mL) alone or combined with EL (25, 50, 75 μM). The full-length Western blot gel images are shown in supplementary files. Values are represented as mean ± SEM of three independent experiments (n = 3), with $^{*}P \leq 0.05$, $^{**}P \leq 0.01$, and $^{***}P \leq 0.001$ indicating statistical significance.

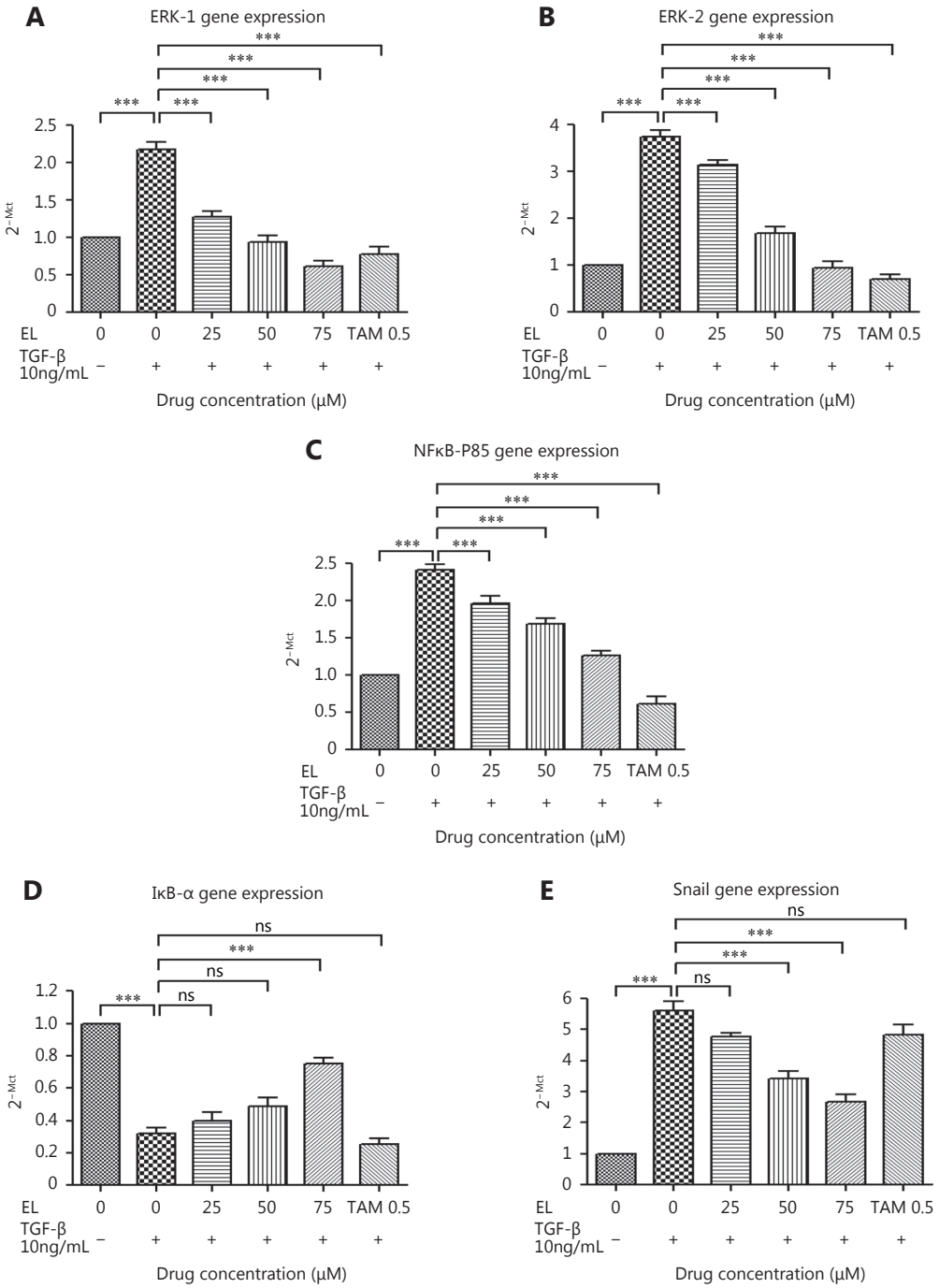

Figure 6 EL on the levels of ERK-1/2, NF-κB/p65, IκB-α and Snail gene expression. (A) Increased gene expression of ERK-1 after TGF-β stimulation, and decreased ERK-1 gene expression with 25, 50, and 75 μM of EL treatments, in a dose dependent manner. (B) Increased gene expression of ERK-2 after TGF-β stimulation, and decreased ERK-2 gene expression with 25, 50, and 75 μM of EL treatments, in a dose dependent manner. (C) Increased gene expression of NF-κB/p65 after TGF-β stimulation and decreased NF-κB/p65 gene expression with 25, 50, and 75 μM of EL treatments, in a dose dependent manner. (D) Decreased gene expression of IκB-α after TGF-β stimulation, and increased IκB-α gene expression with 25, 50, and 75 μM of EL treatments, in a dose dependent manner. (E) Increased gene expression of Snail after TGF-β stimulation, and decreased Snail gene expression with 25, 50, and 75 μM of EL treatments, in a dose dependent manner. Values are represented as mean ± SEM of three independent experiments (n = 3), with *$P \leq 0.05$, **$P \leq 0.01$, and ***$P \leq 0.001$ indicating statistical significance.

compared with the untreated cells, whereas EL treatment at concentrations of 25, 50, and 75 μM resulted in significant decreases of ~2- ($P \leq 0.01$), ~1.7-, and ~1.3-fold, respectively ($P \leq 0.001$), compared with only TGF-β-treated cells. TAM treatment (0.5 μM) also resulted in a significant decrease of ~0.6-fold ($P \leq 0.001$) in NF-κB/p65 gene expression compared with only TGF-β-treated cells. We also studied the effects of EL on an NF-κB inhibitor, inhibitor κB-α (IκB-α), where TGF-β stimulation was found to significantly inhibit IκB-α gene expression to ~0.3-fold ($P \leq 0.001$) compared with the untreated cells, and EL was found to significantly increase IκB-α gene expression to ~0.75-fold only when 75 μM EL ($P \leq 0.001$) was used, compared with only TGF-β-treated cells (**Figure 6D**). No significant change in the expression was observed following TAM treatment. Finally, Snail gene expression was also increased very significantly (~5.6-fold) after TGF-β stimulation, and was significantly suppressed to ~3.4- and ~2.7-fold when concentrations of 50 and 75 μM EL were used, respectively ($P \leq 0.001$), compared with only TGF-β-treated cells (**Figure 6E**). However, no significant change in Snail gene expression was observed following TAM treatment.

These finding were confirmed by the changes in protein level expression due to EL treatment in MDA-MB-231 cells undergoing TGF-β-induced EMT. As shown in **Figure 7A**, the total ERK-1/2 (tERK-1/2) protein expression was significantly upregulated (~1.4-folds; $P \leq 0.01$) in the TGF-β-stimulated cells compared with the untreated cells. However, tERK-1/2 protein expression was significantly downregulated to ~0.8-, ~0.6-, and 0.4-fold when concentrations of 25, 50, and 75 μM EL were used ($P \leq 0.001$) with TGF-β induction, compared with only TGF-β-induced cells. A significant decrease (~0.7-fold) was observed in tERK-1/2 protein expression when 0.5 μM TAM was used ($P \leq 0.001$), compared with only TGF-β-treated cells. We also investigated the effects of EL on the phosphorylation of ERK-1/2 (pERK-1/2), where a significant increase of ~1.9-fold ($P \leq 0.001$) was observed in pERK-1/2 protein expression with TGF-β stimulation, compared with the untreated cells. In contrast, a significant decrease in pERK-1/2 protein expression to ~1.3-, ~0.9-, and ~0.8-fold was observed when concentrations of 25, 50, and 75 μM EL were used, respectively, compared with only TGF-β-treated cells (**Figure 7B**). A significant decrease (~1-fold) was observed when a concentration of 0.5 μM TAM was used ($P \leq 0.001$) compared with only TGF-β-treated cells. NF-κB/p65 protein expression also increased very significantly (~1.5-fold) after TGF-β stimulation, and was significantly suppressed to ~0.8-, ~0.7-, and ~0.6-fold when concentrations of 25, 50, and 75 μM EL were used, respectively ($P \leq 0.001$), compared with only TGF- β-treated cells (**Figure 7C**). TAM also significantly reduced NF-κB/p65 protein expression to ~1.2-fold ($P \leq 0.05$) compared with only TGF- β-treated cells. Similar results were observed in the case of Snail (**Figure 7D**), where a significant increase to ~1.5-fold ($P \leq 0.01$) in protein expression was observed after TGF-β stimulation, compared with the untreated cells, and significant decreases to ~0.7-, ~0.6-, and ~0.4-fold were observed when concentrations of 25, 50, and 75 μM EL were used, respectively ($P \leq 0.001$), compared with only TGF- β-treated cells. There was significant decrease to ~0.8-fold when 0.5 μM TAM was used ($P \leq 0.001$), compared with only TGF-β-treated cells. Briefly, we confirmed that EL reverted TGF-β-induced EMT in MDA-MB-231 breast cancer cells *in vitro* by inhibiting the ERK/NF-κB/Snail pathway at the mRNA and protein levels.

Discussion

Metastasis is the leading cause of death and treatment failure in breast cancer patients. EMT is the primary process in the metastatic cascade which plays crucial role in tumor recurrence and metastasis along with cancer stem cells (CSCs) in breast cancer[20]. During EMT in cancer cells, well-organized and tightly connected epithelial cells transdifferentiate into disorganized and motile mesenchymal cells through the induction of an engineered, reversible transcriptional program. This program is identified by the disruption of the tight junctions between epithelial cells caused by the downregulation and delocalization of tight junction proteins zonula occludens-1 (ZO-1), occludin, and claudin, and the dissolution of adherens cell junction complexes containing E-cadherin, p120-catenin, γ-catenin, and β-catenin[5,21,22]. This leads to the subsequent loss of apical-basal cell polarity, dramatic remodeling of the cytoskeleton, and the formation of actin stress fibers. Concomitantly, the cells acquire mesenchymal features such as a spindle-shaped fibroblast-like morphology, and express mesenchymal components including N-cadherin, vimentin, fibronectin, and alpha smooth-muscle actin[12]. Cortical organization of actin filaments is an another hallmark of epithelial cells, whereas cells undergoing EMT reorganize their cortical actin cytoskeleton by forming actin stress fibers in order to acquire mesenchymal properties such as dynamic cell elongation and directional motility[12,23]. Thus, EMT is also characterized by increased cell contractility and actin stress fiber formation. Recent evidence suggests the possible role of MAPK-p38 and CD44 in the control of actin stress fibers formation, which might contribute to the modulation of cell motility and the invasive phenotype of cancer cells

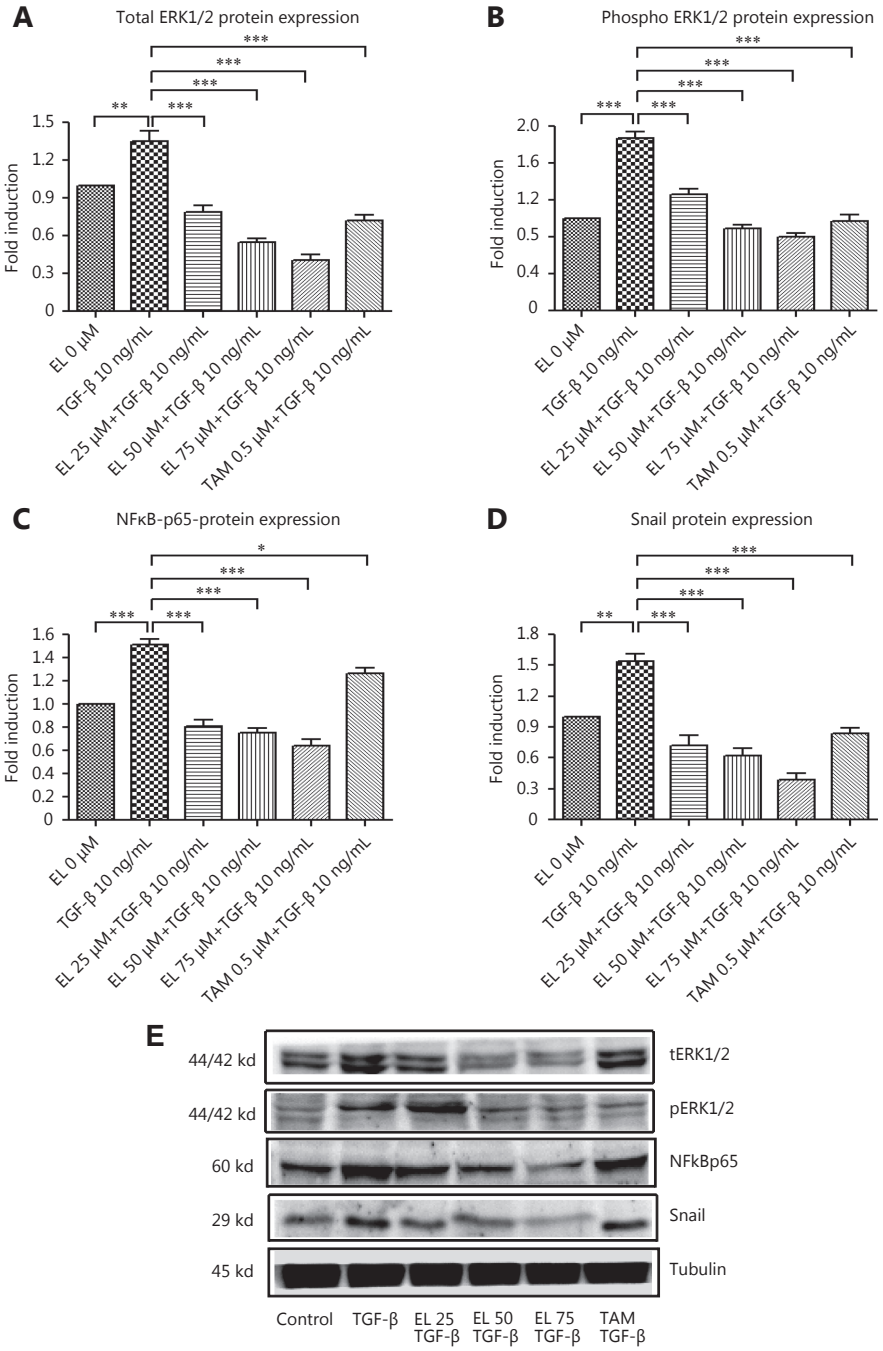

Figure 7 Effects of EL on the levels of ERK-1/2, NF-κB/p65, and Snail protein expression. (A) Increased protein expression of tERK-1/2 after TGF-β stimulation, and decreased tERK-1/2 protein expression with 25, 50, and 75 μM of EL treatments, in a dose dependent manner. (B) Increased protein expression of pERK-1/2 after TGF-β stimulation, and decreased pERK-1/2 protein expression with 25, 50, and 75 μM of EL treatments, in a dose dependent manner. (C) Increased protein expression of NF-κB/p65 after TGF-β stimulation, and decreased NF-κB/p65 protein expression with 25, 50, and 75 μM of EL treatments, in a dose dependent manner. (D) Increased protein expression of Snail after TGF-β stimulation, and decreased Snail protein expression with 25, 50, and 75 μM of EL treatments, in a dose-dependent manner. (E) Representative Western blot results for the tERK-1/2, pERK-1/2, NF-κB/p65, and Snail proteins derived from cells treated with TGF-β (10 ng/mL) alone or combined with EL (25, 50, 75 μM). The full-length Western blot gel images are shown in supplementary files. Values are represented as mean ± SEM of three independent experiments (n =3), with *P ≤ 0.05, **P ≤ 0.01, and ***P ≤ 0.001 indicating statistical significance.

undergoing EMT[24-26]. All these molecular processes coerce the cancer cells undergoing EMT to develop increased motility and the invasive phenotype, and undergo metastasis during cancer progression.

Recent advances in breast cancer research have provided new insights into the molecular mechanisms and different signaling pathways underlying EMT initiation and regulation during breast cancer progression and metastasis[9,27-29]. As mentioned earlier, TGF-β1 is one of the leading metastasis inducers, and promotes EMT by transcriptional and posttranscriptional regulation of a group of transcription factors that suppress epithelial features and enhance mesenchymal features in various cancers, including breast cancer[4,13,21,27,30]. Thus, TGF-β signaling has been shown to play an important role in EMT; indeed, adding TGF-β to epithelial cells in culture is a convenient way of inducing EMT in various epithelial cells[21]. TGF-β acts through both Smad-dependent and Smad-independent pathways that overlap and function together to regulate several transcription factors including Snail, Slug, and Twist[9,31], which function as master molecular switches in the EMT program. The functional loss of E-cadherin—a key cell–cell adhesion molecule—is a hallmark of EMT. Snail was the first transcription repressor of E-cadherin to be discovered, and is now considered one of the most important transcription factors that regulate the EMT[8,32]. Snail plays a fundamental role in EMT and breast cancer metastasis by suppressing E-cadherin expression, and its overexpression has been found in both the epithelial and endothelial cells of invasive breast cancer, but is undetectable in the normal breast[33,34]. The expression of Snail in breast carcinomas is associated with metastasis, tumor recurrence, and poor prognosis[35,36]. It has been reported that during TGF-β-induced EMT, Snail forms a transcriptional repressor complex with Smad3/4 that targets the adjacent E-boxes and Smad-binding elements in genes encoding junction proteins such as E-cadherin, coxsackievirus and Ad receptor (CAR), and occludin. This results in the repression of epithelial genes and the induction of genes associated with the mesenchymal and invasive phenotype, such as *FN* and *MMP9*[37,38]. However, another transcription factor—NF-κB—also plays an essential role in the induction and maintenance of TGF-β-induced EMT[10]. The NF-κB pathway regulates Snail expression via transcriptional and post-translational mechanisms, where NF-κB/p65 undergoes nuclear translocation, binds to the human Snail promoter, and increases Snail transcription[8,10,39]. Thus NF-κB acts as an upstream regulator of Snail in TGF-β-induced EMT associated with breast cancer progression. Moreover, ERK and MAPKs have been proposed as key mediators in TGF-β signaling, and several studies have indicated that ERK signals may repress considerable subsets of intermediate TGF target genes by transmodulating and regulating some regulators of transcription in Smad cascades[40,41]. Previous studies have demonstrated that TGF-β1 induces the activation of the ERK signaling pathway, which is required for TGF-β1-mediated EMT *in vitro*[42], and this activation of the ERK pathway contributes to the regulation of NF-κB activity during TGF-β-induced EMT in breast cancer metastasis[10]. Briefly, the ERK/NF-κB/Snail signaling pathway plays an important role in TGF-β-induced EMT, which leads to breast cancer metastasis, and targeting this pathway to revert EMT is a novel and attractive therapeutic strategy for combatting breast cancer metastasis.

ED and EL—the mammalian lignans derived from the flax lignan—are known for their anti-breast cancer activity, and their antimetastatic potential has been reported in several animal and human breast cancer xenograft studies[14]. Several *in vitro* cell culture studies have also demonstrated some of the cellular and molecular mechanisms of ED and EL in different breast cancer cell lines affecting various cellular behaviors, such as adhesion, invasion, and migration, during metastasis[43-46]. Recent studies have shown the ability of EL to inhibit FAK-Src signaling and uPA/Plasmin/MMP signaling to suppress migration and metastasis in lung cancer and breast cancer cell lines, respectively[16,47]. In our previous work, we demonstrated the antimetastatic potential of EL via its several mechanisms, such as the repression of MMP2 and MMP9 gene and protein expression, the alteration of the filopodia and lamellipodia structures of the actin cytoskeleton, and the inhibition of proliferation, migration, and ECM remodeling through the blockade of uPA/Plasmin/MMP signaling[15,16]. A previous study has confirmed that TGF-β1 enhances the invasive properties of MDA-MB-231 breast cancer cells by upregulating uPA activity[48]. Owing to this background, we hypothesized the possible role of EL in TGF-β-induced EMT, and investigated the changes to the ERK/NF-κB/Snail signaling pathway in MDA-MB-231 breast cancer cells upon EMT induction following EL treatment *in vitro*.

In the present study, we report new molecular mechanisms underlying the antimetastatic potential of EL, which contribute to the inhibition of TGF-β-induced EMT by interfering with the ERK/NF-κB/Snail signaling pathway in MDA-MB-231 breast cancer cells. We investigated the cellular functional consequences of TGF-β-induced EMT in MDA-MB-231 breast cancer cells, and the effects of EL on these functional consequences using cell migration and cell invasion assays. Our findings suggest that TGF-β significantly

increased the migratory and invasive potential of the cells compared with the untreated control cells, indicating increased cellular functional malignancy due to the induction of EMT. However, EL treatment elicited a dose-dependent reduction in the migration and invasion of cells undergoing TGF-β-induced EMT compared with only TGF-β-stimulated cells *in vitro*. In order to investigate the molecular mechanisms behind the augmented cellular functional malignancy as a consequence of TGF-β-induced EMT, we demonstrated that EL significantly suppressed the expression of ERK, NF-κB/p65, and Snail at the mRNA and protein levels. EL significantly suppressed augmented protein expression of both ERK and phosphorylated ERK due to TGF-β1 treatment during EMT induction. Similarly, EL also repressed NF-κB/p65 and Snail at the gene and protein levels by preventing degradation of inhibitor κB-α (IκB-α), which is an NF-κB inhibitor. We found that EL significantly reversed TGF-β-induced EMT by upregulating epithelial markers such as E-cadherin and occludin, and downregulating mesenchymal markers such as vimentin and N-cadherin. EL also revoked TGF-β1-induced reorganization of the cortical actin cytoskeleton by reducing the formation of actin stress fibers in the breast cancer cells. EL significantly reduced the expression of MAPK-p38 and CD44 at the mRNA and protein levels, which resulted in the control of actin stress fiber formation; therefore, EL might contribute to the modulation of cell motility and the invasive phenotype of MDA-MB-231 cells undergoing TGF-β-induced EMT. Briefly, our findings demonstrate a novel effect of EL that could provide a new therapeutic strategy to combat breast cancer metastasis by inhibiting TGF-β-induced EMT via the ERK/NF-κB/Snail signaling pathway (**Figure 8**). The role of the ERK/NF-κB/Snail signaling pathway in TGF-β-induced EMT was evaluated by Strippoli, et al. in 2008; they reported that ERK controls NF-κB nuclear translocation and the transcriptional activity induced by TGF-β1, and the ERK/NF-κB activation pathway regulates Snail1 expression[7]. For the first time they characterized the role of the ERK/NF-κB/Snail signaling pathway in TGF-β1-stimulated EMT, and demonstrated that the blockade of ERK/NF-κB/Snail signaling can reverse TGF-β-induced EMT in peritoneal mesothelial cells. A similar pathway was recently evaluated by Han et al., who described its direct role in the regulation of TGF-β-induced EMT and CSCs in MCF-7 and MDA-MB-231 breast cancer cells[10]. They confirmed their findings by demonstrating the reversal of TGF-β-induced EMT via inhibition of the ERK/NF-κB/Snail signaling pathway by disulfiram (DSF) in breast cancer cells. DSF is a synthetic drug that has been used in the treatment of alcohol use disorders. Increasing evidence suggests that DSF has potential as a potent anticancer drug. In accordance with the effects of DSF on the expression profile of EMT shown by Han et al., EL treatment can also bring about the reversal of TGF-β-induced EMT in the TNBC cell line MDA-MB-231 via modulation of the ERK/NF-κB/Snail signaling pathway. It should be noted that DSF is a synthetic drug and EL is a mammalian lignan derived from dietary lignans. However, both seem to share some common mechanistic features with respect to the above signaling pathway. These features include the inhibition of invasion and migration, and the restoration of the epithelial phenotype by downregulating mesenchymal markers such as vimentin and N-cadherin, and upregulating epithelial markers such as E-cadherin and occludin in the TNBC cell line. It is quite possible that they differ in other anti-breast cancer mechanisms. Despite the fact that both antimetastatic agents share a comparable mechanism, structurally they are very different, and we are currently unable to comment on why two different-looking structures have similar activity. This needs to be studied.

TNBC accounts for about 20% of breast cancers, and is characterized by the absence of estrogen receptor (ER) and progesterone receptor (PR) and the absence of Her2 overexpression[49]. TNBC is more metastatic and invasive than non-TNBC, and its management is challenging because of a lack of targeted therapy, aggressive behavior, and relatively poor prognosis[50]. Currently, chemotherapy is the primary established systemic treatment for TNBC patients in both the early and advanced stages of the disease[51]. Therefore, novel therapeutic strategies and drugs to prevent metastasis are urgently needed. EMT and CSCs are emerging as promising new therapeutic targets for novel cancer therapy[52]. Several drugs and new small molecule inhibitors targeting TGF-β-induced EMT have been identified as clinical therapeutics, and are undergoing pre-clinical and clinical trials in various metastatic cancers including TNBC[53]. Herein we have explored the novel molecular mechanisms of EL with regard to one of the promising therapeutic targets, i.e., TGF-β-induced EMT, and we suggest that EL is a potential antimetastatic molecule for the treatment of metastatic TNBC. Furthermore, to the best of our knowledge, this is the first report of the efficacy of EL with regard to the inhibition of TGF-β-induced EMT by blocking the ERK/NF-κB/Snail signaling pathway in TNBC cells *in vitro*. Additional studies on the various metastasis signaling pathways in breast cancer and clinical studies are warranted to further substantiate the antimetastatic potential of EL.

Conflict of interest statement

No potential conflicts of interest are disclosed.

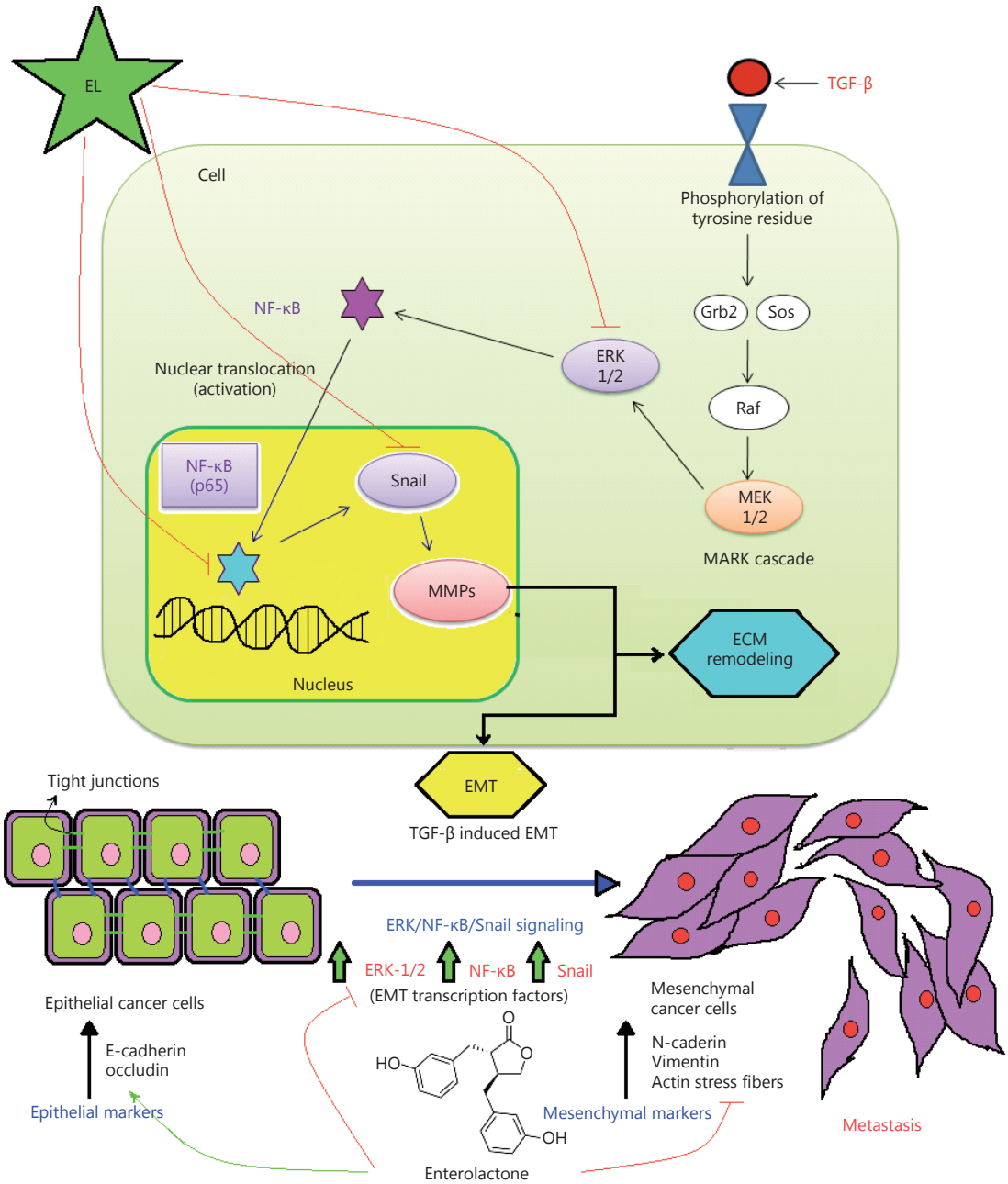

Figure 8 Inhibition of TGF-β-induced EMT in MDA-MB-231 breast cancer cells by blocking the ERK/NF-κB/Snail signaling pathway *in vitro*.

References

1. Torre LA, Bray F, Siegel RL, Ferlay J, Lortet-Tieulent J, Jemal A. Global cancer statistics, 2012. CA Cancer J Clin. 2015; 65: 87-108.
2. Hegde MV, Mali AV, Chandorkar SS. What is a cancer cell? Why does it metastasize? Asian Pac J Cancer Prev. 2013; 14: 3987-9.
3. Venning FA, Wullkopf L, Erler JT. Targeting ECM disrupts cancer progression. Front Oncol. 2015; 5: 224
4. Padua D, Massagué J. Roles of TGFβ in metastasis. Cell Res. 2009; 19: 89-102.
5. Papageorgis P. TGF*β* signaling in tumor initiation, epithelial-to-mesenchymal transition, and metastasis. J Oncol. 2015; 2015: 587193
6. Huber MA, Azoitei N, Baumann B, Grünert S, Sommer A, Pehamberger H, et al. NF-κB is essential for epithelial-mesenchymal transition and metastasis in a model of breast cancer progression. J Clin Invest. 2004; 114: 569-81.
7. Strippoli R, Benedicto I, Pérez Lozano ML, Cerezo A, López-

Cabrera M, del Pozo MA. Epithelial-to-mesenchymal transition of peritoneal mesothelial cells is regulated by an ERK/NF-κB/Snail1 pathway. Dis Model Mech. 2008; 1: 264-74.
8. Wang YF, Shi J, Chai KQ, Ying XH, Zhou BP. The role of snail in EMT and tumorigenesis. Curr Cancer Drug Targets. 2013; 13: 963-72.
9. Wang YF, Zhou BP. Epithelial-mesenchymal transition in breast cancer progression and metastasis. Chin J Cancer. 2011; 30: 603-11.
10. Han D, Wu G, Chang C, Zhu F, Xiao Y, Li QH, et al. Disulfiram inhibits TGF-β-induced epithelial-mesenchymal transition and stem-like features in breast cancer via ERK/NF-κB/Snail pathway. Oncotarget. 2015; 6: 40907-19.
11. Talbot LJ, Bhattacharya SD, Kuo PC. Epithelial-mesenchymal transition, the tumor microenvironment, and metastatic behavior of epithelial malignancies. Int J Biochem Mol Biol. 2012; 3: 117-36.
12. Lamouille S, Xu J, Derynck R. Molecular mechanisms of epithelial-mesenchymal transition. Nat Rev Mol Cell Biol. 2014; 15: 178-96.
13. Heerboth S, Housman G, Leary M, Longacre M, Byler S, Lapinska K, et al. EMT and tumor metastasis. Clin Transl Med. 2015; 4: 6
14. Flower G, Fritz H, Balneaves LG, Verma S, Skidmore B, Fernandes R, et al. Flax and breast cancer: a systematic review. Integr Cancer Ther. 2014; 13: 181-92.
15. Mali AV, Wagh UV, Hegde MV, Chandorkar SS, Surve SV, Patole MV. *In vitro* anti-metastatic activity of enterolactone, a mammalian lignan derived from flax lignan, and down-regulation of matrix metalloproteinases in MCF-7 and MDA MB 231 cell lines. Indian J Cancer. 2012; 49: 181-7.
16. Mali AV, Joshi AA, Hegde MV, Kadam SS. Enterolactone suppresses proliferation, migration and metastasis of MDA-MB-231 breast cancer cells through inhibition of uPA induced plasmin activation and MMPs-Mediated ECM remodeling. Asian Pac J Cancer Prev. 2017; 18: 905-15.
17. Gebäck T, Schulz MMP, Koumoutsakos P, Detmar M. TScratch: a novel and simple software tool for automated analysis of monolayer wound healing assays. Biotechniques. 2009; 46: 265-74.
18. Schmittgen TD, Livak KJ. Analyzing real-time PCR data by the comparative C_T method. Nat Protoc. 2008; 3: 1101-8.
19. Devarajan E, Sahin AA, Chen JS, Krishnamurthy RR, Aggarwal N, Brun AM, et al. Down-regulation of caspase 3 in breast cancer: a possible mechanism for chemoresistance. Oncogene. 2002; 21: 8843-51.
20. Takebe N, Warren RQ, Ivy SP. Breast cancer growth and metastasis: interplay between cancer stem cells, embryonic signaling pathways and epithelial-to-mesenchymal transition. Breast Cancer Res. 2011; 13: 211
21. Xu J, Lamouille S, Derynck R. TGF-β-induced epithelial to mesenchymal transition. Cell Res. 2009; 19: 156-72.
22. Thiery JP, Sleeman JP. Complex networks orchestrate epithelial–esenchymal transitions. Nat Rev Mol Cell Biol. 2006; 7: 131-42.
23. Shankar J, Nabi IR. Actin cytoskeleton regulation of epithelial mesenchymal transition in metastatic cancer cells. PLoS One. 2015; 10: e0119954
24. Chen ZY, Wang PW, Shieh DB, Chiu KY, Liou YM. Involvement of gelsolin in TGF-beta 1 induced epithelial to mesenchymal transition in breast cancer cells. J Biomed Sci. 2015; 22: 90
25. Haynes J, Srivastava J, Madson N, Wittmann T, Barber DL. Dynamic actin remodeling during epithelial-mesenchymal transition depends on increased moesin expression. Mol Biol Cell. 2011; 22: 4750-64.
26. Park GB, Ko HS, Kim D. Sorafenib controls the epithelial-mesenchymal transition of ovarian cancer cells via EGF and the CD44-HA signaling pathway in a cell type-dependent manner. Mol Med Rep. 2017; 16: 1826-36.
27. Taylor MA, Parvani JG, Schiemann WP. The pathophysiology of epithelial-mesenchymal transition induced by transforming growth factor-β in normal and malignant mammary epithelial cells. J Mammary Gland Biol Neoplasia. 2010; 15: 169-90.
28. Roxanis I. Occurrence and significance of epithelial-mesenchymal transition in breast cancer. J Clin Pathol. 2013; 66: 517-21.
29. Sarrió D, Rodriguez-Pinilla SM, Hardisson D, Cano A, Moreno-Bueno G, Palacios J. Epithelial-mesenchymal transition in breast cancer relates to the basal-like phenotype. Cancer Res. 2008; 68: 989-97.
30. Heldin CH, Vanlandewijck M, Moustakas A. Regulation of EMT by TGFβ in cancer. FEBS Lett. 2012; 586: 1959-70.
31. Aomatsu K, Arao T, Sugioka K, Matsumoto K, Tamura D, Kudo K, et al. TGF-β induces sustained upregulation of SNAI1 and SNAI2 through smad and non-smad pathways in a human corneal epithelial cell line. Investig Ophthalmol Vis Sci. 2011; 52: 2437-43.
32. Barrallo-Gimeno A, Nieto MA. The Snail genes as inducers of cell movement and survival: implications in development and cancer. Development. 2005; 132: 3151-61.
33. Parker BS, Argani P, Cook BP, Han LF, Chartrand SD, Zhang M, et al. Alterations in vascular gene expression in invasive breast carcinoma. Cancer Res. 2004; 64: 7857-66.
34. Martin TA, Goyal A, Watkins G, Jiang WG. Expression of the transcription factors snail, slug, and twist and their clinical significance in human breast cancer. Ann Surg Oncol. 2005; 12: 488-96.
35. Peinado H, Olmeda D, Cano A. Snail, Zeb and bHLH factors in tumour progression: an alliance against the epithelial phenotype? Nat Rev Cancer. 2007; 7: 415-28.
36. Wu Y, Zhou BP. TNF-α/NF-κB/Snail pathway in cancer cell migration and invasion. Br J Cancer. 2010; 102: 639-44.
37. Vincent T, Neve EPA, Johnson JR, Kukalev A, Rojo F, Albanell J, et al. A SNAIL1–MAD3/4 transcriptional repressor complex promotes TGF-β mediated epithelial–esenchymal transition. Nat Cell Biol. 2009; 11: 943-50.
38. Wu YD, Zhou BP. Snail: more than EMT. Cell Adh Migr. 2010; 4: 199-203.
39. Barberà MJ, Puig I, Domínguez D, Julien-Grille S, Guaita-Esteruelas S, Peiró S, et al. Regulation of Snail transcription during epithelial to mesenchymal transition of tumor cells. Oncogene. 2004; 23: 7345-54.
40. Yang YC, Piek E, Zavadil J, Liang D, Xie DL, Heyer J, et al.

Hierarchical model of gene regulation by transforming growth factor β. Proc Natl Acad Sci USA. 2003; 100: 10269-74.

41. Ramos C, Becerril C, Montaño M, García-De-Alba C, Ramírez R, Checa M, et al. FGF-1 reverts epithelial-mesenchymal transition induced by TGF-β1 through MAPK/ERK kinase pathway. Ame J Phys Lung Cell Mol Physiol. 2010; 229: L222-31.
42. Xie L, Law BK, Chytil AM, Brown KA, Aakre ME, Moses HL. Activation of the Erk pathway is required for TGF-β1-induced EMT *in vitro*. Neoplasia. 2004; 6: 603-10.
43. Chen JM, Thompson LU. Lignans and tamoxifen, alone or in combination, reduce human breast cancer cell adhesion, invasion and migration *in vitro*. Breast Cancer Res Treat. 2003; 80: 163-70.
44. Wang LD, Chen JM, Thompson LU. The inhibitory effect of flaxseed on the growth and metastasis of estrogen receptor negative human breast cancer xenograftsis attributed to both its lignan and oil components. Int J Cancer. 2005; 116: 793-8.
45. Magee PJ, McGlynn H, Rowland IR. Differential effects of isoflavones and lignans on invasiveness of MDA-MB-231 breast cancer cells *in vitro*. Cancer Lett. 2004; 208: 35-41.
46. Xiong XY, Hu XJ, Li Y, Liu CM. Inhibitory effects of enterolactone on growth and metastasis in human breast cancer. Nutr Cancer. 2015; 67: 1326-34.
47. Chikara S, Lindsey K, Borowicz P, Christofidou-Solomidou M, Reindl KM. Enterolactone alters FAK-Src signaling and suppresses migration and invasion of lung cancer cell lines. BMC Complement Altern Med. 2017; 17: 30
48. Farina AR, Coppa A, Tiberio A, Tacconelli A, Turco A, Colletta G, et al. Transforming growth factor-β1 enhances the invasiveness of human MDA-MB-231 breast cancer cells by up-regulating urokinase activity. Int J Cancer. 1998; 75: 721-30.
49. Collignon J, Lousberg L, Schroeder H, Jerusalem G. Triple-negative breast cancer: treatment challenges and solutions. Breast Cancer. 2016; 8: 93-107.
50. Liu YP, Zhu PT, Wang YY, Wei ZH, Tao L, Zhu ZJ, et al. Antimetastatic therapies of the polysulfide diallyl trisulfide against triple-negative breast cancer (TNBC) via suppressing MMP2/9 by blocking NF-κB and ERK/MAPK signaling pathways. PLoS One. 2015; 10: e0123781
51. Bianchini G, Balko JM, Mayer IA, Sanders ME, Gianni L. Triple-negative breast cancer: challenges and opportunities of a heterogeneous disease. Nat Rev Clin Oncol. 2016; 13: 674-90.
52. Kwon M. Epithelial-to-mesenchymal transition and cancer stem cells: emerging targets for novel cancer therapy. Cancer Gene Ther. 2014; 21: 179-80.
53. Kothari AN, Mi ZY, Zapf M, Kuo PC. Novel clinical therapeutics targeting the epithelial to mesenchymal transition. Clin Transl Med. 2014; 3: 35

Cite this article as: Mali AV, Joshi AA, Hegde MV, Kadam SS. Enterolactone modulates the ERK/NF-κB/Snail signaling pathway in triple-negative breast cancer cell line MDA-MB-231 to revert the TGF-β-induced epithelial–mesenchymal transition. Cancer Biol Med. 2018; 15: 137-56. doi: 10.20892/j.issn.2095-3941.2018.0012

Table S1 List of oligonucleotide primers synthesized for real time PCR

Gene	Forward primer	Reverse primer
N-cadherin	5′-ATTGGACCATCACTCGGCTTA-3′	5′-CACACTGGCAAACCTTCACG-3′
Occludin	5′-TCAGGGAATATCCACCTATCACTTCAG-3′	5′-CATCAGCAGCAGCCATGTACTCTTCAC-3′
CD44	5-GACACCATGGACAAGTTTTGG-3	5-CGGCAGGTTATATTCAAATCG-3
MAPK-p38	5′-GAAGAGCCTGACCTACGAT-3′	5′- ACTGCCAAGGAGCATCTA-3′
ERK-1	5′-CCTGCGACCTTAAGATTTGTGATT-3′	5′-CAGGGAAGATGGGCCGGTTAGAGA-3′
ERK-2	5′-GCGCGGGCCCGGAGATGGTC-3′	5′-TGAAGCGCAGTAAGATTTTT-3′
NF-κB/p-65	5′-GACCTGAATGCTGTGCGG C-3′	5′-ATCTTGAGCTCGGCAGTGTT-3′
IκB-α	5′-CACTCCATCCTGAAGGCTACCAA-3′	5′-AAGGGCAGTCCGGCCATTA-3′
Snail	5′-TCTAGGCCCTGGCTGCTACAA-3′	5′-ACATCTGAGTGGGTCTGGAGGTG-3′
GAPDH	5′-TTTTTGGTTGAGCACAGG-3′	5′-TCAAGTTCCTTCATCCATTC-3′

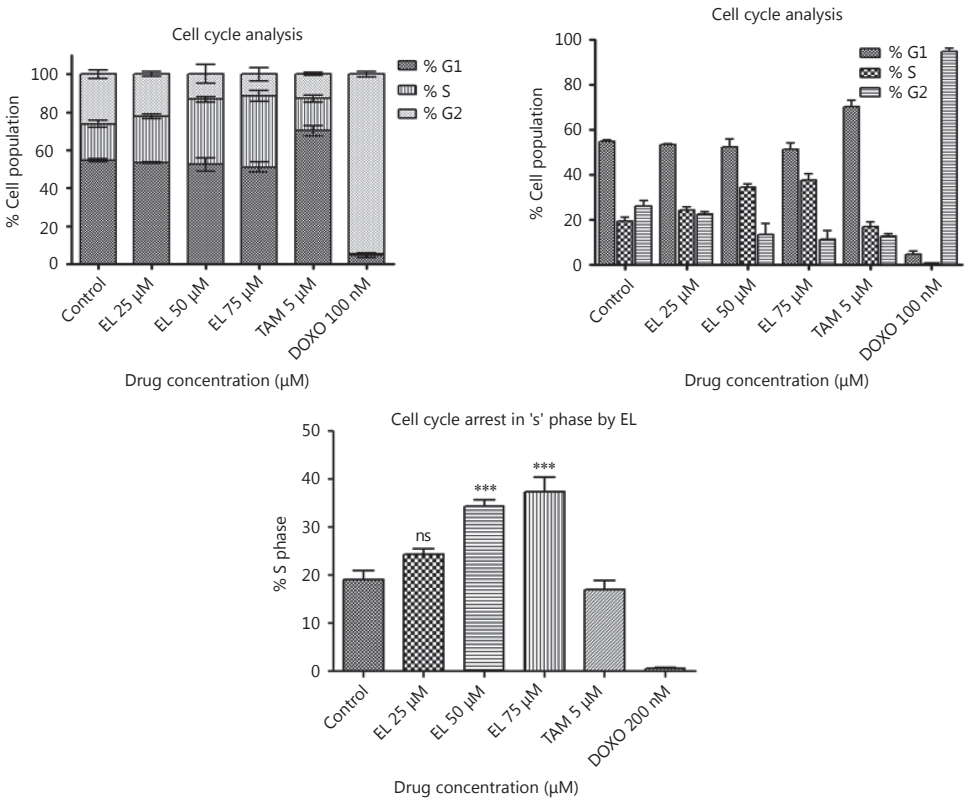

Figure S1 Cell cycle arrest in ‘S’ phase by increasing concentrations of EL. Effects of EL, TAM and DOXO on cell cycle of MDA-MB-231 cells representing % of cell population in each phase upon 48 h of treatment.

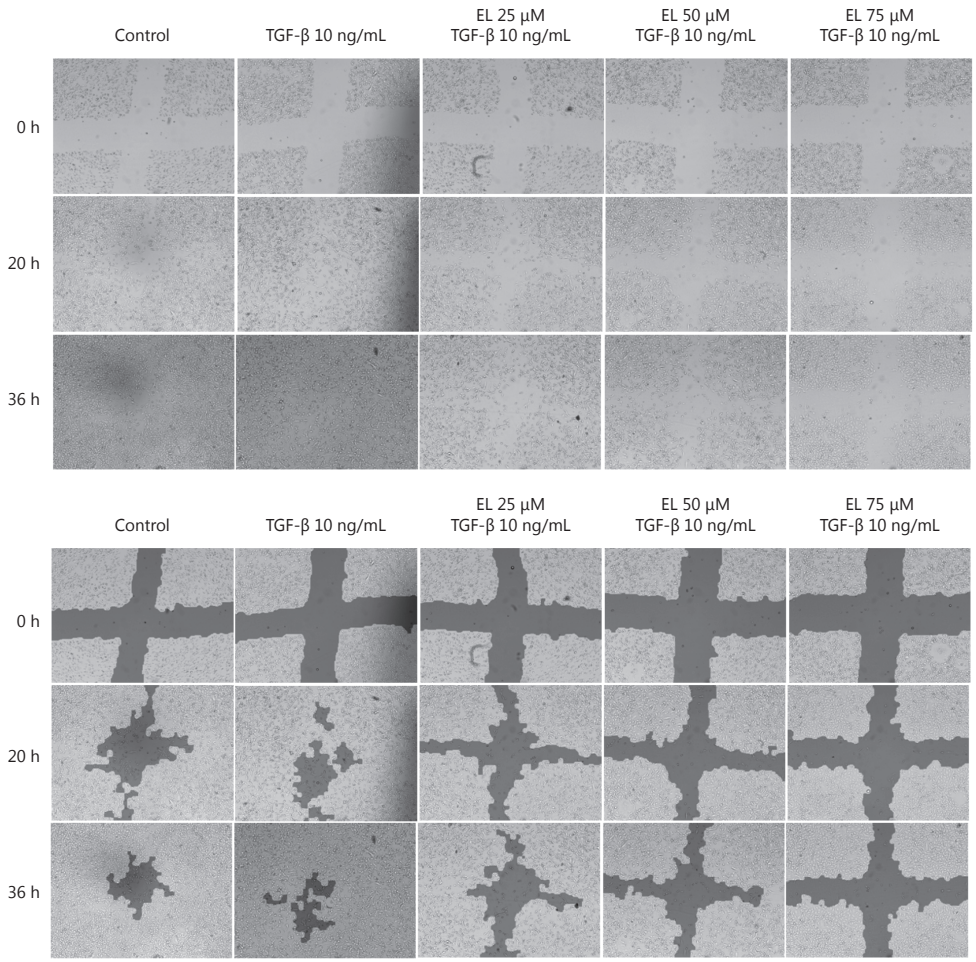

Figure S2 The original, unprocessed images of the cell migration assay were presented as follows and same images processed with a computational tool; TScratch software were shown in the manuscript

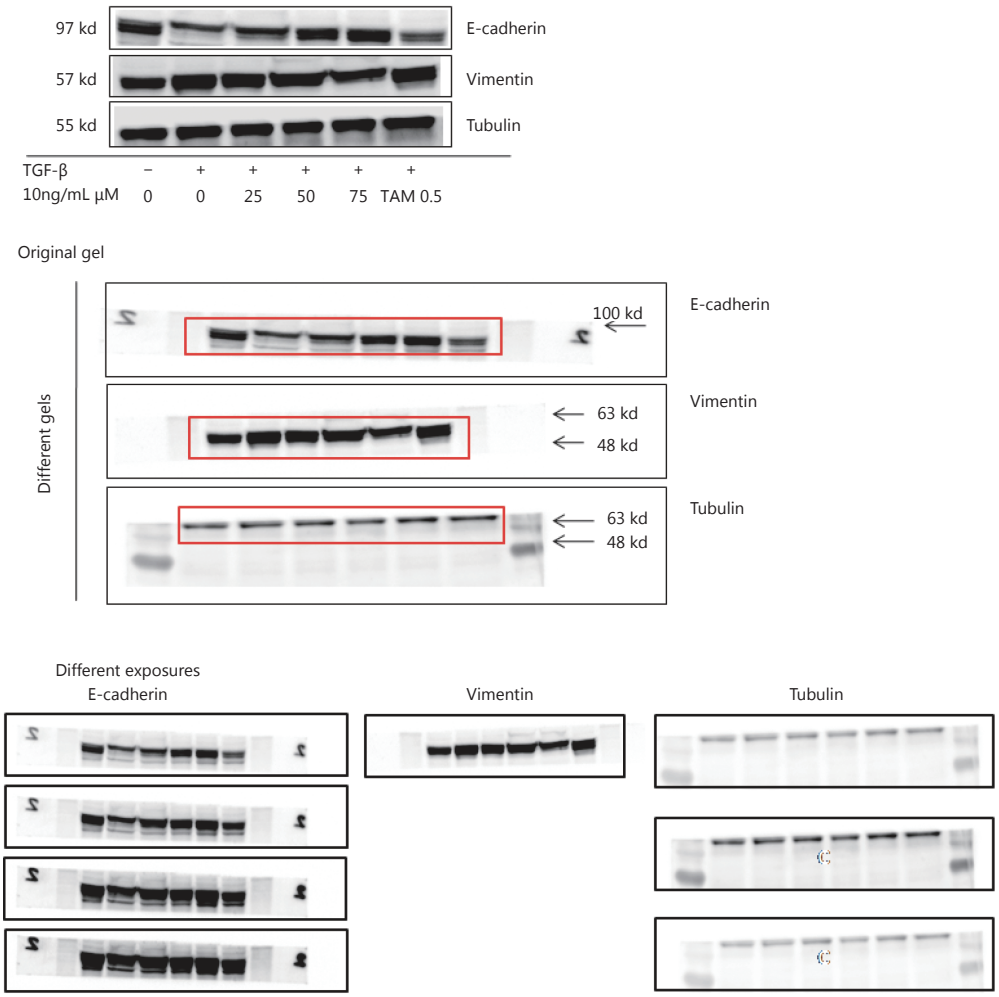

Figure S3 The full length Western blot images and the results in the red frames are shown in the manuscript.

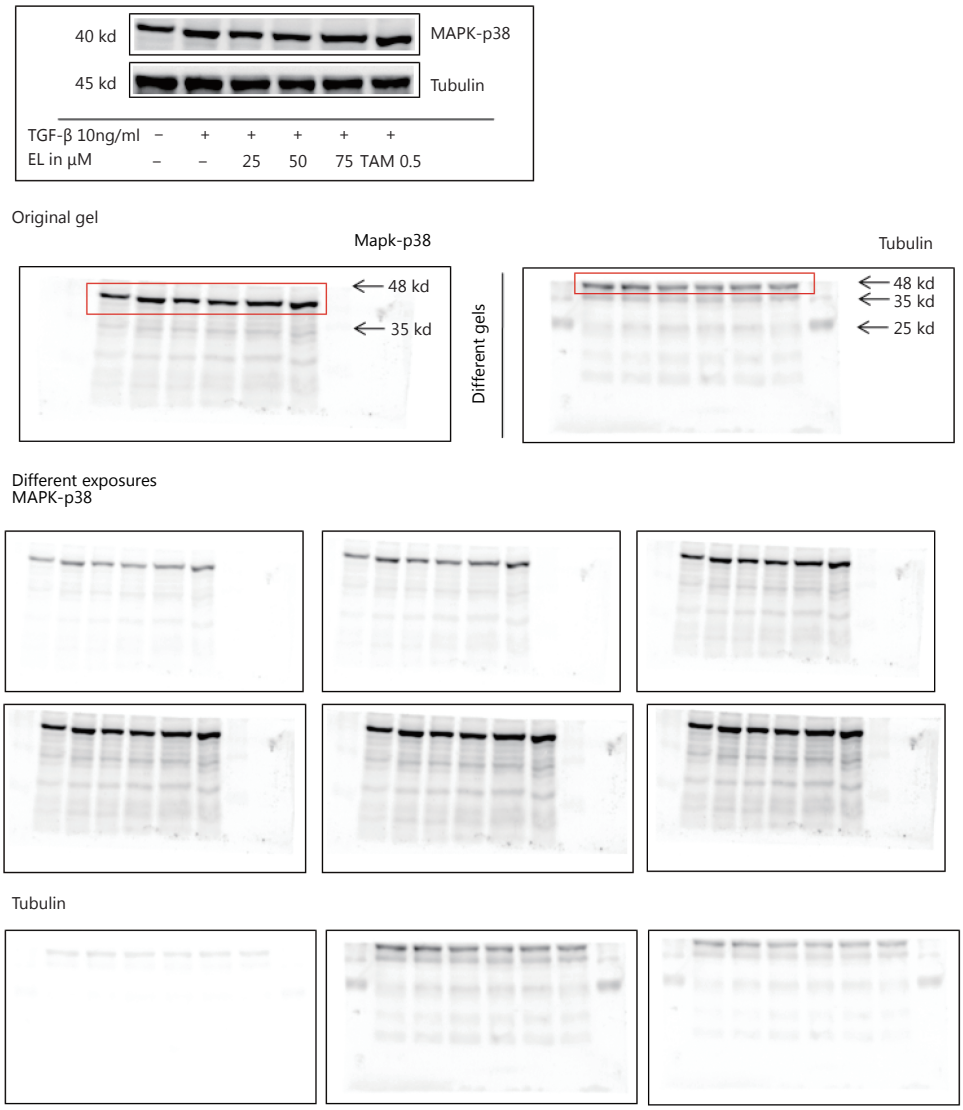

Figure S4 The full length Western blot images and the results in the red frames are shown in the manuscript.

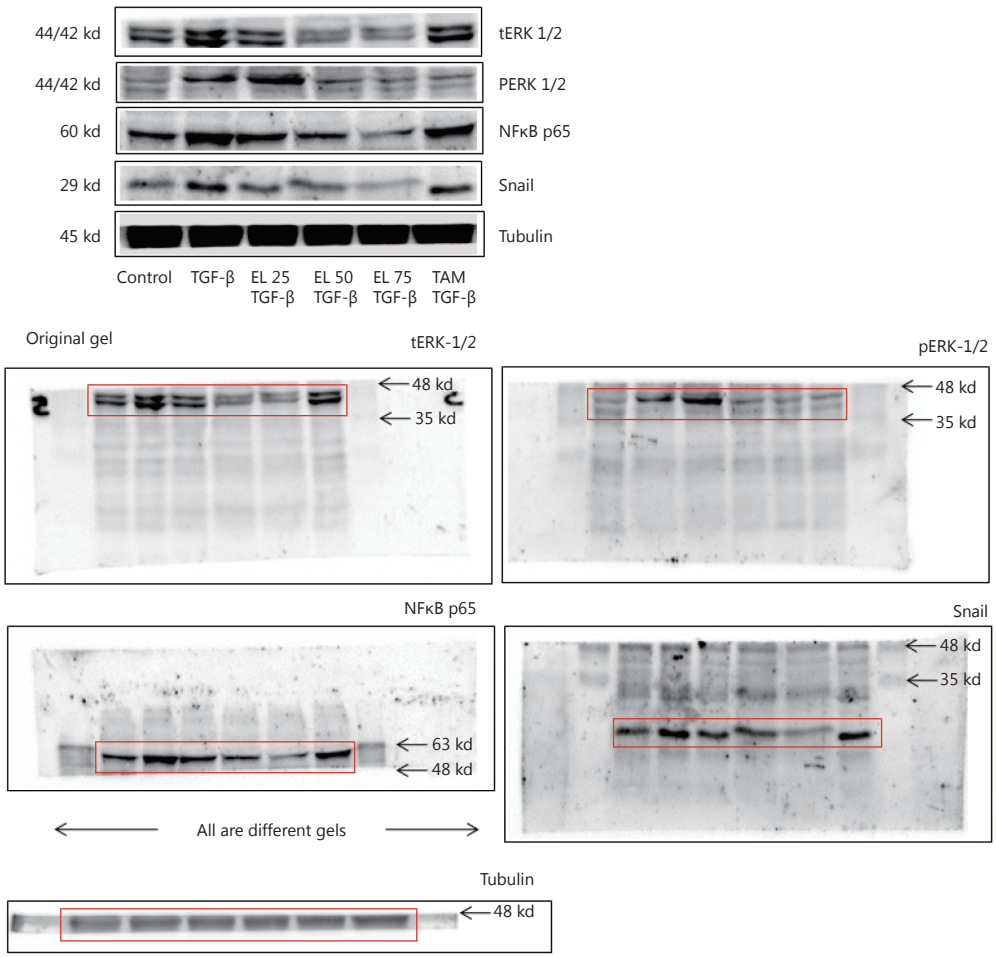
44/42 kd
tERK 1/2
44/42 kd
PERK 1/2
60 kd
NFκB p65
29 kd
Snail
45 kd
Tubulin
Control
TGF-β
EL 25 TGF-β
EL 50 TGF-β
EL 75 TGF-β
TAM TGF-β
Original gel
tERK-1/2
48 kd
35 kd
pERK-1/2
48 kd
35 kd
NFκB p65
63 kd
48 kd
Snail
48 kd
35 kd
All are different gels
Tubulin
48 kd

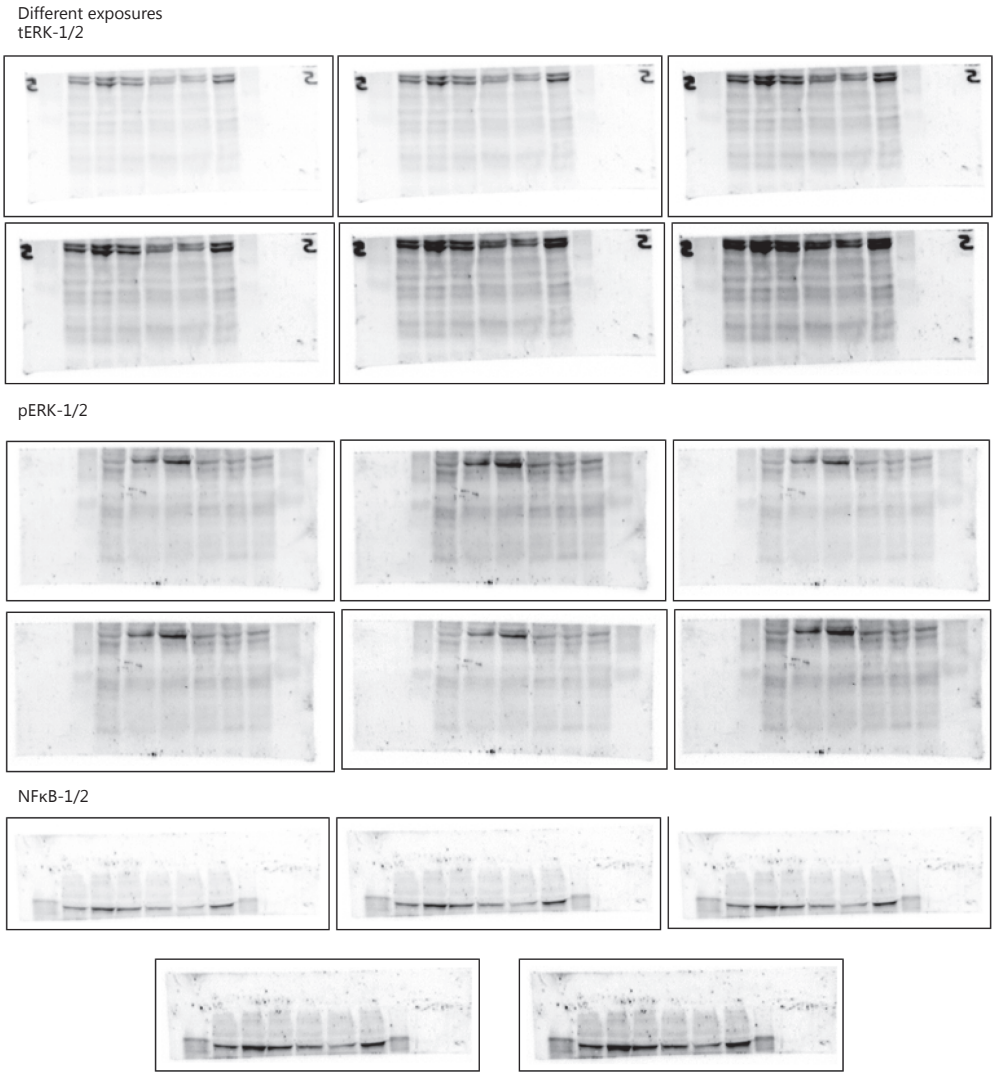
Different exposures
tERK-1/2
pERK-1/2
NFκB-1/2

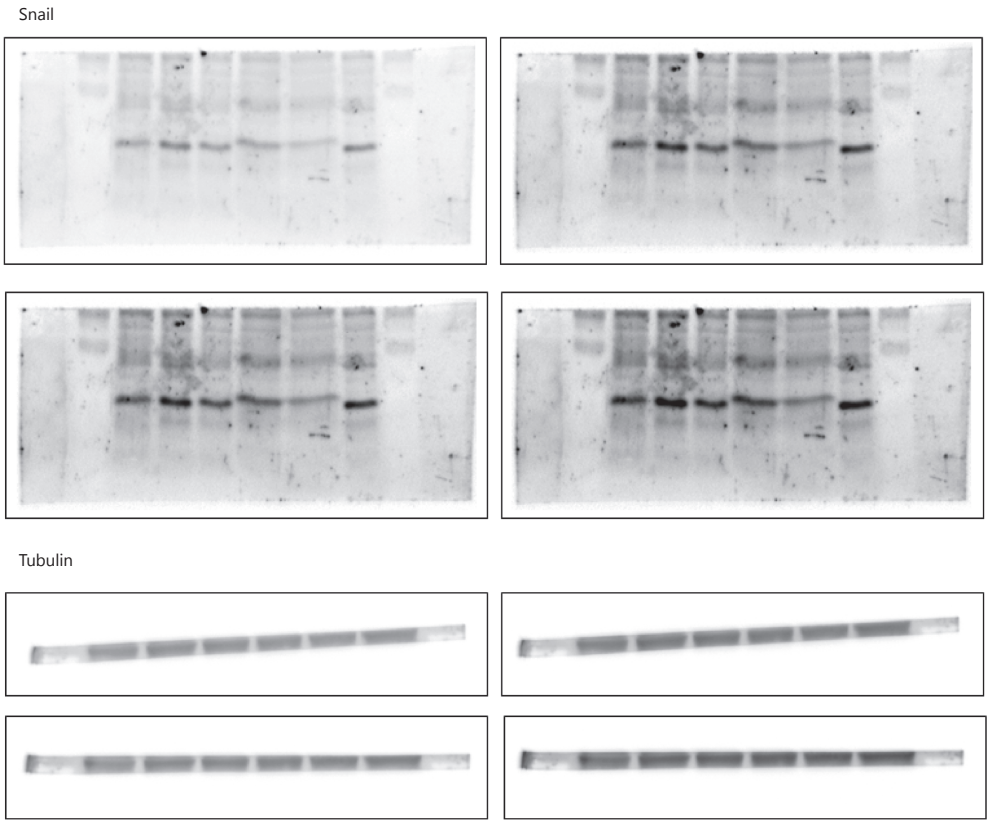

Figure S5 The full length Western blot images and the results in the red frames are shown in the manuscript.